CHAPETR FOUR

EXPERIMENTAL RESULS AND DISCUSSIONS

4.1 General

The experimental program outlined in the preceding chapter was directed to serve two purposes. The first purpose is to investigate the mechanical properties of nanosilica reactive powder concrete (NSRPC) including compressive strength f'_{cf}, splitting tensile strength f_{spf}, modulus of rupture f_{rf} and modulus of elasticity E_{cf} . To achieve this aim, control specimens were prepared from nine different mixes of NSRPC and were tested at the age of 28 days . In these mixes, three main "material" parameters were varied; namely, percentage of nanosilica NS, percentage of silica fume SF and percentage of steel fibers V_f. Results of the control specimens tests and a comprehensive discussion of the effect of each of these three material parameters on the mechanical properties of NSRPC are given in the first part of this chapter.

The second purpose of the experimental program is to investigate the structural performance and shear capacity of sixteen simply supported beams made from such new concrete (referred to as NSRPC beams). These beams were categorized into seven groups and were all designed to fail in shear. In addition to the three mentioned material parameters, NSRPC beams of the present investigation also had three more variable "beam" parameters. These are the longitudinal steel reinforcement ratio ρ, shear span to effective depth ratio a/d and the presence of steel stirrups. Results of the experimental tests on these beams and a comprehensive discussion of the effect of each individual "material"

and "beam" parameter on the shear performance of any tested group of beams are given in the second part of this chapter.

For each tested beam, the diagonal cracking load, ultimate shear capacity, cracking pattern , crack width, mode of failure, strain variation and load – deflection behaviour are all pointed out and discussed.

4.2 Effects of Material Parameters on the Mechanical Properties of NSRPC

4.2.1 Effect of Nanosilica (Group 1)

The variation of the percentage of nanosilica (NS) in NSRPC mixes is found to have pronounced effects on the compressive strength f'_{cf}, splitting tensile strength f_{spf} , modulus of rupture f_{rf} and modulus of elasticity E_{cf} of the hardened concrete as shown in Table 4.1 and Figs. 4.1, 4.2, 4.3 and 4.4 respectively .Four different mixes of NSRPC are considered, designated as $M_{0,15,2}$, $M_{1,15,2}$, $M_{2,15,2}$, $M_{3,15,2}$ containing NS=0%, 1%, 2% and 3% respectively, with constant percentages of silica fume was15% and that of steel fibers was2%.

Table 4.1 summarizes the effects of changing NS on the mechanical properties of concrete. Mix $M_{0,15,2}$ is the reference mix with which the results of the other three mixes are compared.

Table 4.1 reveals that when nanosilica content was increased from zero to 1%, 2% and 3%, the respective percentage increases in the mechanical properties of NSRPC were as follows:

-Compressive Strength f'_{cf} increased by 15.3%, 26.7% and 31.3% respectively.

-Splitting Tensile Strength f_{spf} increased by 29.7%,41.3%and45.3% respectively.

Table 4.1: Effect of Nanosilica on the Mechanical Properties of NSRPC

Mix Designation	*NS%*	*SF%*	*V_f %*	*Compressive Strength f'_{cf} (MPa)*		*Splitting Tensile Strength f_{spf} (MPa)*		*Modulus of Ruptue f_{rf} (MPa)*		*Modulus of Elasticity E_{cf} (GPa)*	
				Value	*% Increase*	*Value*	*% Increase*	*Value*	*% Increase*	*Value*	*% Increase*
$M_{0,15,2}$ *Reference mix*	0	15	2	120	-	17.2	-	19	-	47.81	-
$M_{1,15,2}$	1	15	2	138.3	15.3	22.3	29.7	25.8	35.8	51.04	6.8
$M_{2,15,2}$	2	15	2	152	26.7	24.3	41.3	27.7	45.8	53.3	11.5
$M_{3,15,2}$	3	15	2	157.6	31.3	25	45.3	28.5	50	54.21	13.4

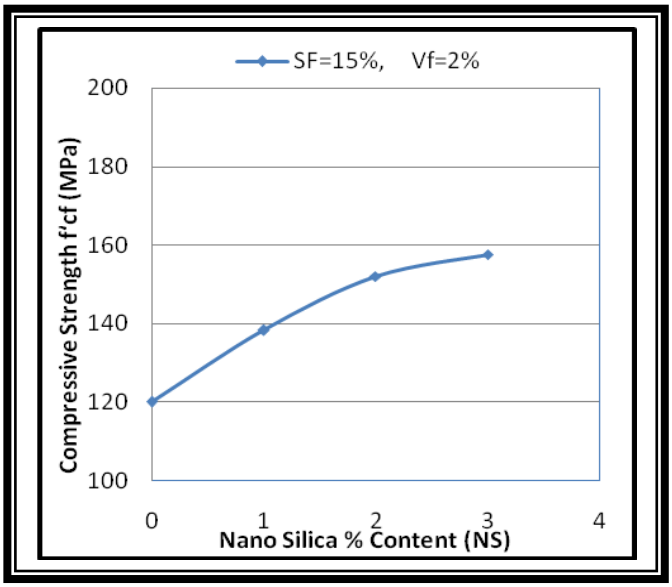

Fig. 4.1 :Effect of Varying Percentage of Nanosilica on Compressive Strength

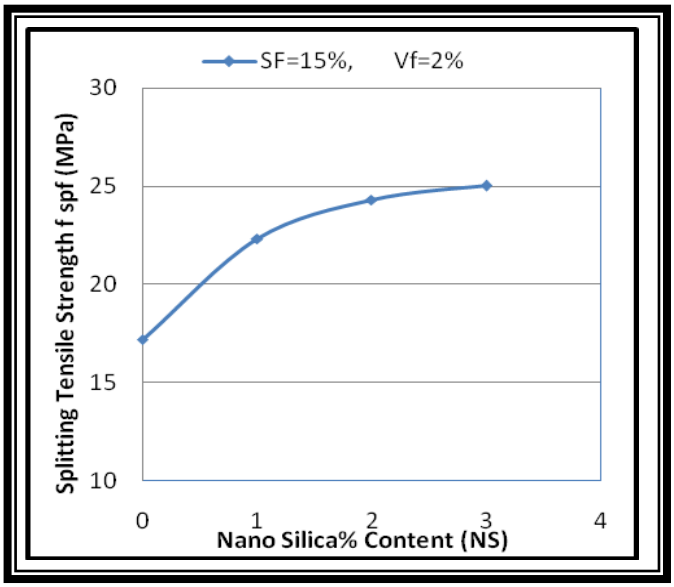

Fig. 4.2 :Effect of Varying Percentage of Nanosilica on Splitting Tensile Strength

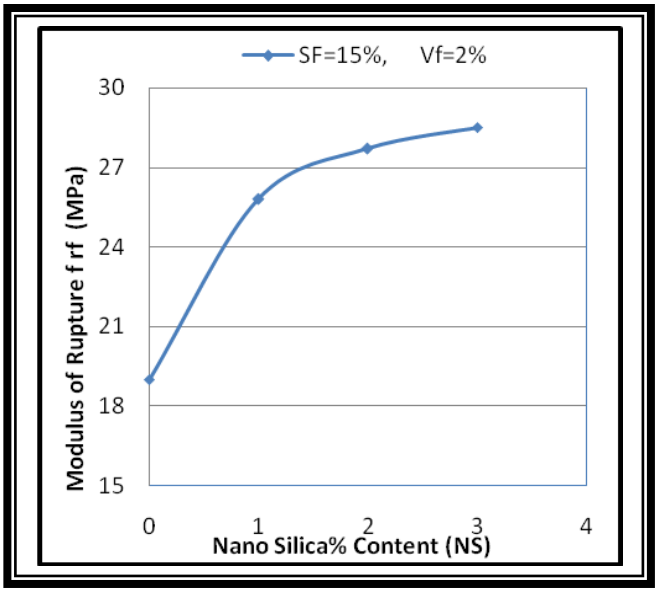

Fig. 4.3 :Effect of Varying Percentage of Nanosilica on Modulus of Rupture

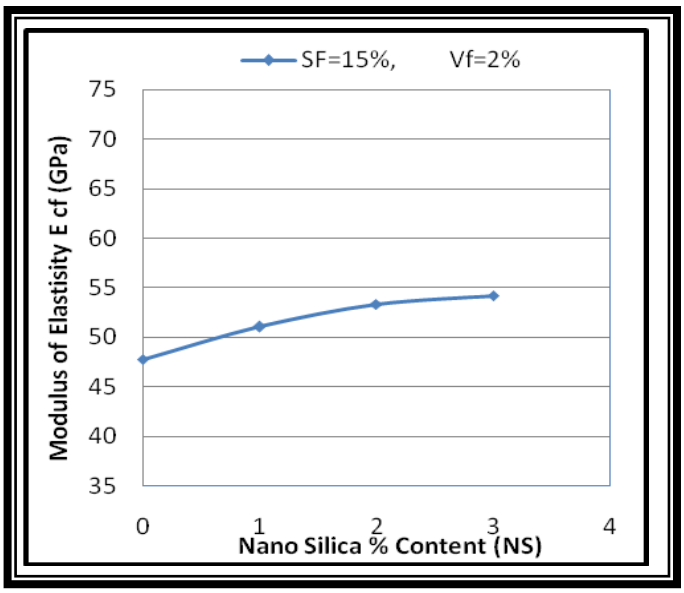

Fig. 4.4: Effect of Varying Percentage of Nanosilica on Modulus of Elasticity

-Modulus of Rupture f_{rf} increased by 35.8%, 45.8% as 50% respectively.

-Modulus of Electricity E_{cf} increased by 6.8%,11.5% and 13.4% respectively.

It can be seen from Figs. 4.1 to 4.4 that the increase in each individual mechanical property with the percentage increase in NS is non-linear and of the convex shape. This means that higher percentages of NS can only add little enhancement to the value of the specified mechanical property, and an optimum percentage of NS was found to be 3%.

The compressive strength improvement due to nanosilica increase in a mix can be attributed to a 4-stage mechanism which improves the infrastructure and consequently increases mechanical properties of the concrete. As a result of this mechanism the following are concluded:

1. Pozzolanic reaction [70,71]: A large amount of calcium hydroxide crystals is produced during the cement–water reaction (Eqs.(1) and (2)). Crystals of $Ca(OH)_2$ are a hexagonal crystals which exist in the transition area between the aggregates and the cement paste matrix and are harmful for strength and durability of concrete.

   Nanosilica, due to its high special surface, is so reactive and produces C-S-H condensed gel as a result of reaction with $Ca(OH)_2$. Therefore, in the pozzolanic reaction, crystals of $Ca(OH)_2$ decrease and high-strength dense gel C-S-H , (which is a product of pozzolanic reaction, Eq. 3). Increases the density of transition region area by filling empty spaces and thus increases the strength.

   $2C_3S + 11H_2O \rightarrow C\text{-}S\text{-}H + 3Ca(OH)_2$……(1)

   $2C_3S + 9H_2O \rightarrow C\text{-}S\text{-}H + Ca(OH)_2$……(2)

   $2SiO_2 + 3Ca(OH)_2 \rightarrow 3CaO \cdot 2SiO_2 \cdot H_2O$……...(3)

   To further explain the fast reactivity of nanosilica particles it can be said that for nanosilica with unsaturated bonds the reaction process between SiO_2 is as follows (Eqs.4,5 and 6) [72]:

≡Si-O- + H-OH →≡Si-OH..... (4)

≡Si- + H-OH → ≡Si-OH……..(5)

≡Si-OH +$Ca(OH)_2$ →C-S-H……(6)

Thus silica nano-particles undergo quick reactions.

2. Nano-filling property [70]: C-S-H constitutes 70% of hydration product. The average diameter of particles of C-S-H gel is around 10 nm [2]. Nanoparticle, having filling ability property, fills the porosity in C-S-H gel and makes a denser adhesive cement paste.
3. Acting as a nucleus [73,74]: In the structure of the C-S-H gel, nanoparticles can act like nucleus forming an extremely strong bond with C-S-H gel particles. Thus, hydration products' stability increases and mechanical properties and durability of the concrete are expected to improve.
4. Crystal- making control [75]: If the amount of nanoparticles and their spacing is suitable formation process of crystals like $Ca(OH)_2$ in the transition area decreases and cement paste matrix, thus, becomes smoother and denser.

The increase of splitting tensile strength f_{spf} and modulus of rupture f_{rf} due to increase in nanosilica can be attributed to the larger contact area between fibers and mortar resulting in more friction and higher performance of the concrete.

4.2.2. Effect of Silica Fume (Group 2)

Table 4.2 gives summary of the effects of varying SF on the mechanical properties of concrete. It indicates that increasing SF has lesser amount of enhancement in the mechanical properties of the hardened NSRPC compared to that of NS.

Three different mixes of NSRPC are considered, designated as $M_{3,5,2}$, $M_{3,10,2}$ and $M_{3,15,2}$ containing SF=5%, 10% and 15% respectively, with constant percentages of nonosilica NS=3% and steel fibers V_f=2%.

The mix $M_{3,5,2}$ is selected as the reference mix with which the results of the other two mixes are compared. In this way, proper assessments of the enhancements in the mechanical properties (f'_{cf}, f_{spf}, f_{rf} and E_{cf}) of the hardened concrete caused by using higher percentages of silica fume in the mix are obtained as shown in Table 4.2 and Figs. 4.5, 4.6, 4.7 and 4.8 respectively.

Table 4.2 shows that when silica fume content was increased from 5% to 10% and 15% the respective percentage increases in the mechanical properties of NSRPC were as follows:

-Compressive Strength f'_{cf} increased by 5.8 and 12.1% respectively.

- Splitting Tensile Strength f_{spf} increased by 2.6% and 7.8% respectively.

-Modulus of Rupture f_{rf} increased by 6.3% and 12.2% respectively.

-Modulus of Elasticity E_{cf} increased by 2.6% and 5.4% respectively .

The amounts of increase in the values of the mechanical properties due to increase in the percentage of SF are shown in Figs. 4.5 to 4.8. It can be seen from these figures that such enhancements are lesser than those obtained by increasing NS.

The beneficial effect of SF in a mix, despite its minor impotence, can be attributed to two reasons according to Silica Fume User's Manual [59]

1. Particle packing of micro filling as silica fume particles fill spaces between cement grains.
2. Chemical contribution of silica fume as it reacts with Ca (OH)2 to form additional binder material called calcium silicate hydrate, which is very similar to the calicium silicate hydrate from Portland cement hydration.

Table (4-2): Effect of Silica Fume of the Mechanical Properties of NSRPC

Mix Designation	*NS%*	*SF%*	*V_f%*	*Compressive strength f'_{cf} (MPa)*		*Splitting Tensile Strength f_{spf} (MPa)*		*Modulus of Rupture f_{rf} (MPa)*		*Modulus of elasticity E_{cf} (GPa)*	
				Value	*% Increase*	*Value*	*% Increase*	*Value*	*% Increase*	*Value*	*% Increase*
$M_{3,5,2}$ *Reference*	3	5	2	140.6	-	23.2	-	25.4	-	51.42	-
$M_{3,10,2}$	3	10	2	148.7	5.8	23.8	2.6	27	6.3	52.77	2.6
$M_{3,15,2}$	3	15	2	157.6	12.1	25	7.8	28.5	12.2	54.21	5.4

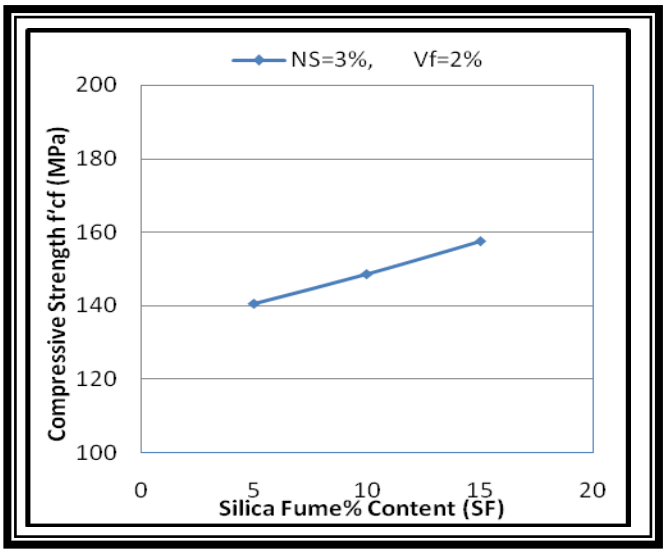

Fig. 4.5: Effect of Varying Percentage of Silica Fume on Compressive Strength

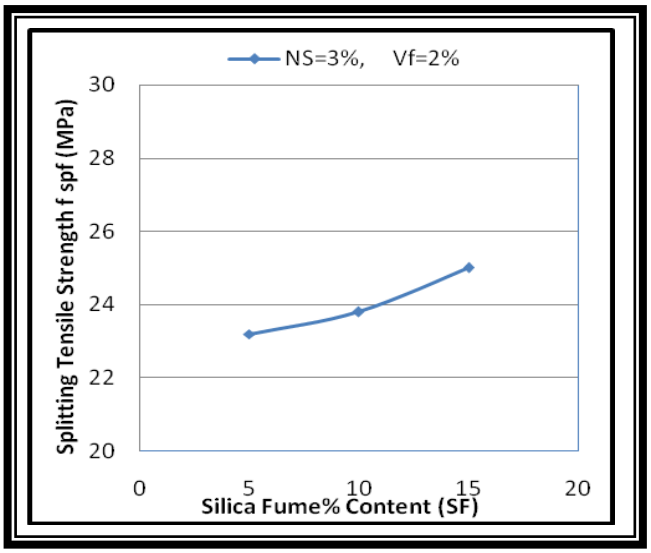

Fig. 4.6 :Effect of Varying Percentage of Silica Fume on Splitting Tensile Strength

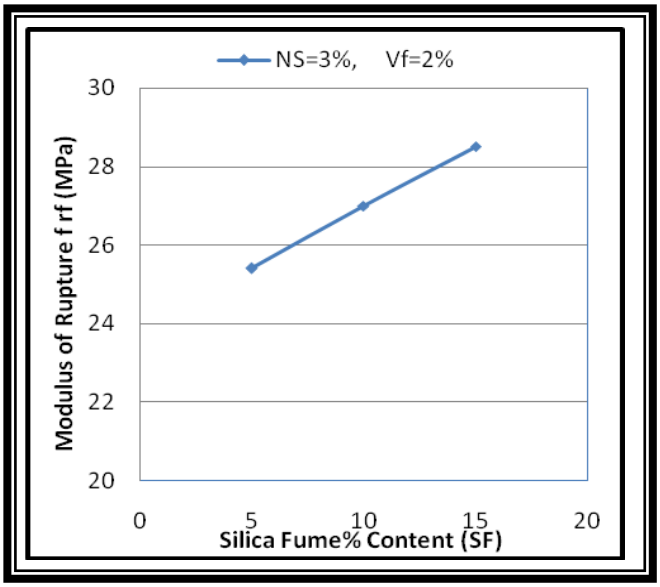

Fig. 4.7 :Effect of Varying Percentage of Silica Fume on Modulus of Rupture

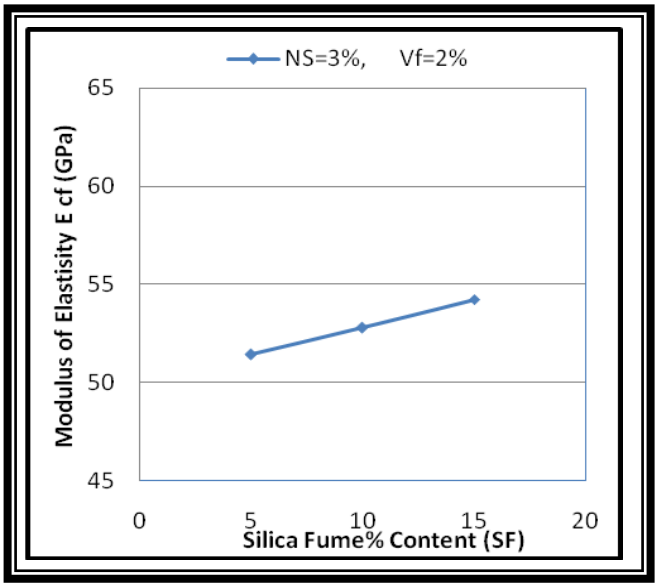

Fig. 4.8: Effect of Varying Percentage of Silica Fume on Modulus of Elasticity

4.2.3 Effect of Steel Fibers (Group 3)

Increasing the percentage of steel fibers (V_f) in NSRPC mixes has resulted in profound enhancements in the mechanical properties f'_{cf}, f_{spf}, f_{rf} and E_{cf} , of the hardened concrete as shown in Table 4.3 and Figs. 4.9, 4.10, 4.11 and 4-12 respectively.

Three different mixes of NSRPC are considered , designated as $M_{3,15,0}$,$M_{3,15,1}$ and $M_{3,15,2}$ containing V_f=0%, 1% and 2% respectively, with constant percentages of nanosilica NS=3% and silica fume SF=15%. The mix $M_{3,15,0}$ is selected as the reference mix with which the results of the other two mixes are compared.

Table 4.3 shows that when the percentage of steel fibers V_f was increased from 0% to 1% and 2%, the respective percentage increases in the mechanical properties of NSRPC were as follows :

-Compressive Strength f'_{cf} increased by 30.6% and 60.8% respectively.

-Splitting Tensile Strength f_{spf} increased by 145.2% and 242.5% respectively.

- Modulus of Rupture f_{rf} increased by 155.3% and 275% respectively.

- Modulus of Elasticity E_{cf} increased by 10.9% and 24.4% respectively.

The amounts of increase in the values of the mechanical properties due to increase in the percentage of V_f are shown in Figs. 4.9 to 4.12. Figure 4.9 shows that increasing V_f caused moderate increases in the compressive strength f'_{cf} while according to Fig. 4.12 it only caused little enhancement in the modulus of elasticity Ec. But Figs. 4.10 and 4.11 show respectively very significant increases in the splitting tensile strength f_{spf} and modulus of rupture f_{rf} caused by increasing V_f.

The increase in compressive strength does likely reflect the contribution of steel fibers to the tensile capacity of NSRPC. An accepted view is that concrete under uniaxial compressive load fails because of lateral strain induced by Poisson's ratio effects leading to lateral swelling of unconfined central section accompanied by cracking parallel to the loading axis and shear failure near the specimen ends. In the nonfibrous NSRPC specimens the compression failure occurred suddenly and violently like an explosion with a high sound and the concrete was splintered. In contrast to the nonfibrous NSRPC specimens, the presence of steel fibers in NSRPC has directed the brittle failure mode of the nonfibrous NSRPC specimens towards a more ductile failure.

The considerable increases in the splitting tensile strength f_{spf} and modulus of rupture f_{rf} of NSRPC due to increase in V_f are similar to those obtained by other investigators like AL-Kadhi[76], Danha[77] and Mahdi[78] on RPC, who all found that using 2% V_f can approximately double f_{spf} and f_{rf}. This is due to the fact that fibers bridge tensile cracks and retard their propagation, as well as transmit stress across a crack, and counteract crack growth.

The slight increases in the modulus of elasticity E_{cf} due to increase in V_f could be attributed to the fact that a higher load was found possible to apply before the concrete matrix can crack. Only thereafter would steel fibers start sharing the resistance of stress with the matrix by interfacial bond between the steel fibers and the matrix.

Table 4.3: Effect of Steel Fibers of the Mechanical Properties of NSRPC

Mix Designation	*NS%*	*SF%*	*Vf%*	*Compressive Strength f'_{cf} (MPa)*		*Splitting Tensile Strength f_{spf} (MPa)*		*Modulus of Rupture f_{rf} (MPa)*		*Modulus of Elasticity E_{cf} (GPa)*	
				Value	*% Increase*	*Value*	*% Increase*	*Value*	*% Increase*	*Value*	*% Increase*
$M_{3,15,0}$ *Reference mix*	3	15	0	98	-	7.3	-	7.6	-	43.59	-
$M_{3,15,1}$	3	15	1	128	30.6	17.9	145.2	19.4	155.3	48.36	10.9
$M_{3,15,2}$	3	15	2	157.6	60.8	25	242.5	28.5	275	54.21	24.4

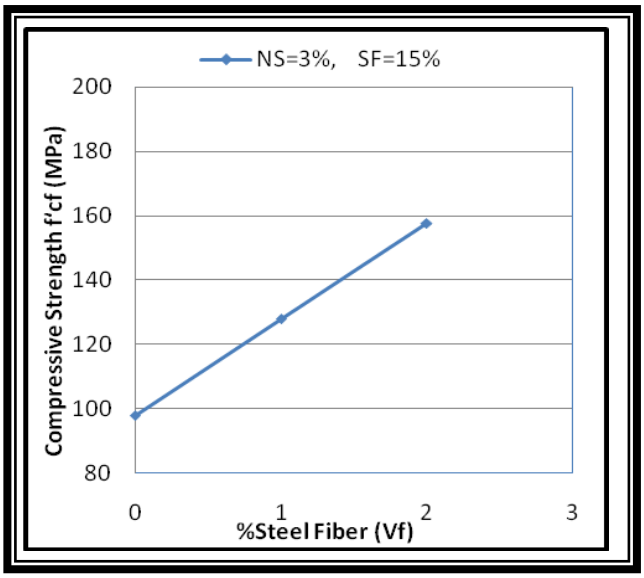

Fig. 4.9: Effect of Varying Percentage of Steel Fibers on Compressive Strength

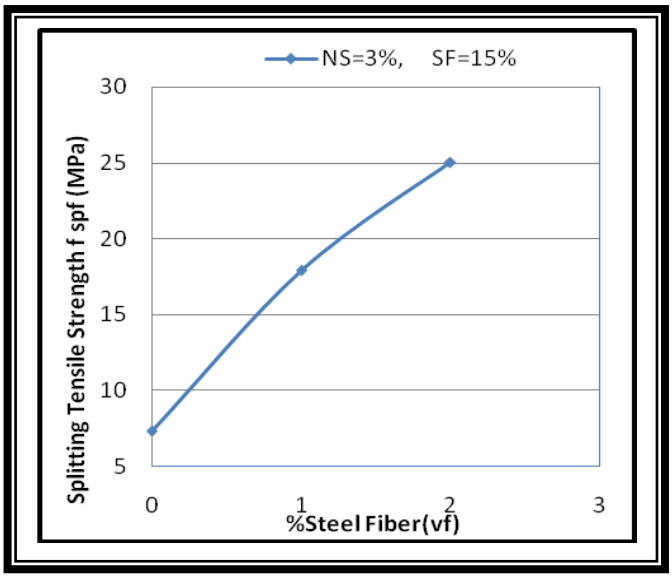

Fig. 4.10: Effect of Varying Percentage of Steel Fibers on Splitting Tensile Strength

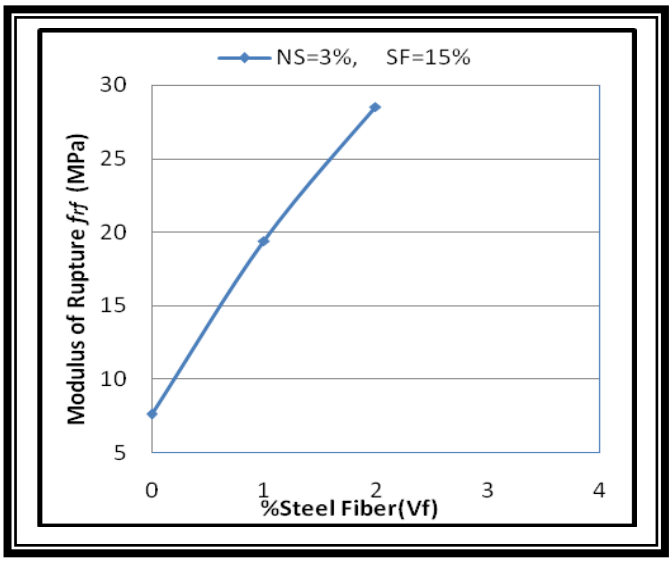

Fig. 4.11: Effect of Varying Percentage of Steel Fibers on Modulus of Rupture

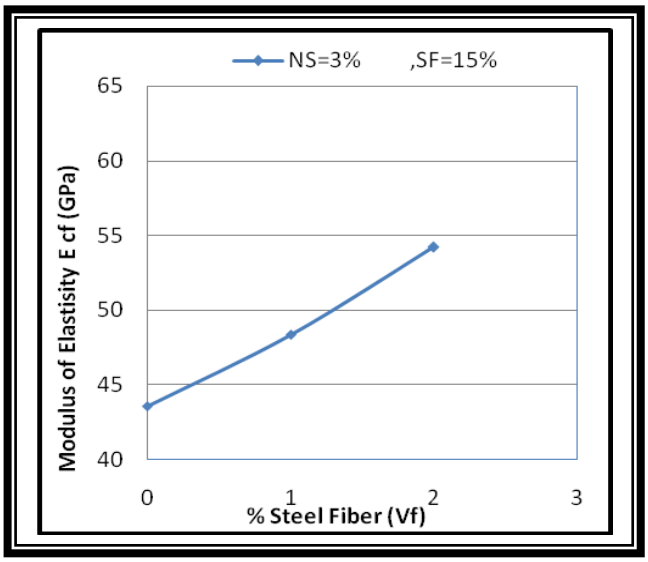

Fig. 4.12: Effect of Varying Percentage of Steel Fibers on Modulus of Elasticity

4.2.4 Effect of the Dual Absence of Nanosilica and Steel Fibers (Group 7)

It is now clear that the two material parameters, nanosilica and steel fibers play significantly major role in the enhancement of any mechanical property of NSRPC. Therefore it is thought useful in the present research to stand on the actual percentage of reduction in the mechanical properties f'_{cf} , f_{spf} , f_{rf} and E_{cf} of concrete due to the dual absence of these two material parameters from the mix.

For this purpose , a mix designated $M_{0,15,0}$ (having NS=0%, SF=15% and V_f=0%) was made whose test results were compared with those of the reference mix $M_{3,15,2}$ (having NS=3%, SF=15% and V_f=2%) in Table 4.4. The two mixes $M_{0,15,0}$ and $M_{3,15,2}$ are referred to as "group 7" in Table 3.1 of Chapter Three.

The values of the mechanical properties f'_{cf}, f_{spf}, f_{rf} and E_{cf} of the hardened concrete of this group are also shown in Figs. 4.13, 4.14, 4.15 and 4.16 respectively .

Table 4.4 reveals that when both nanosilica and steel fibers were absent from the mix, the mechanical properties of the hardened concrete were decreased dramatically such that:

- Compressive Strength f'_{cf} decreased by 52.4%
-Splitting Tensile Strength f_{spf} decreased by 78.8%
-Modulus of Rupture f_{rf} decreased by 81.1%
-Modulus of Elasticity E_{cf} decreased by 28.8%

The actual values of these mechanical properties are shown in Figs. 4.13 to 4.14 in their two phases of presence and dual absence of NS and V_f.

Table 4.4: Effect of Dual Absence of Nanosilica and Steel Fibers on the Mechanical Properties of NSRPC

Mix Designation	*NS%*	*SF%*	*Vf%*	*Compressive Strength f'_{cf} (MPa)*		*Splitting Tensile Strength f_{spf} (MPa)*		*Modulus of Rupture f_{rf} (MPa)*		*Modulus of Elasticity E_{cf} (GPa)*	
				Value	*% Decrease*	*Value*	*% Decrease*	*Value*	*% Decrease*	*Value*	*% Decrease*
$M_{3,15,2}$ *Reference mix*	3	15	2	157.6	-	25	-	28.5	-	54.21	-
$M_{0,15,0}$	0	15	0	75	52.4	5.3	78.8	5.4	81.1	38.6	28.8

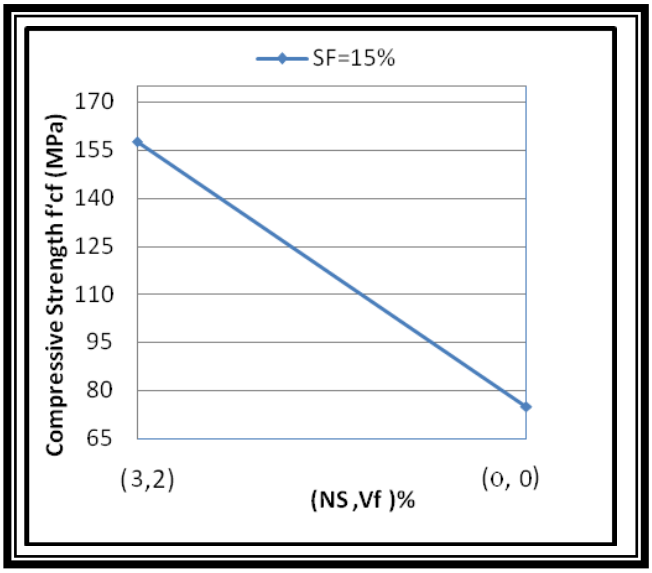

Fig. 4.13: Effect of Dual Absence of Nanosilica and Steel Fibers on Compressive Strength

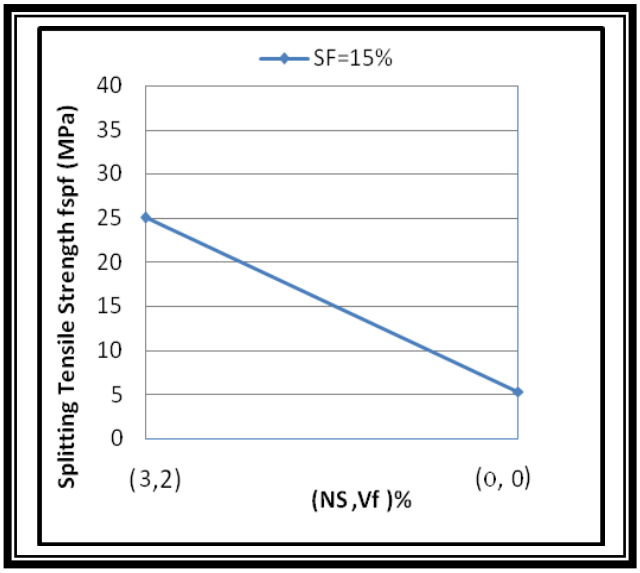

Fig. 4.14: Effect of Dual Absence of Nanosilica and Steel Fibers on Splitting Tensile Strength

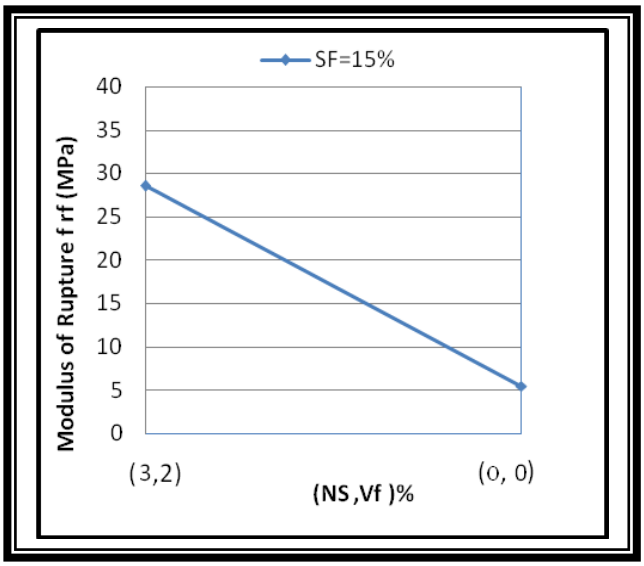

Fig. 4.15: Effect of Dual Absence of Nanosilica and Steel Fibers on Modulus of Rupture

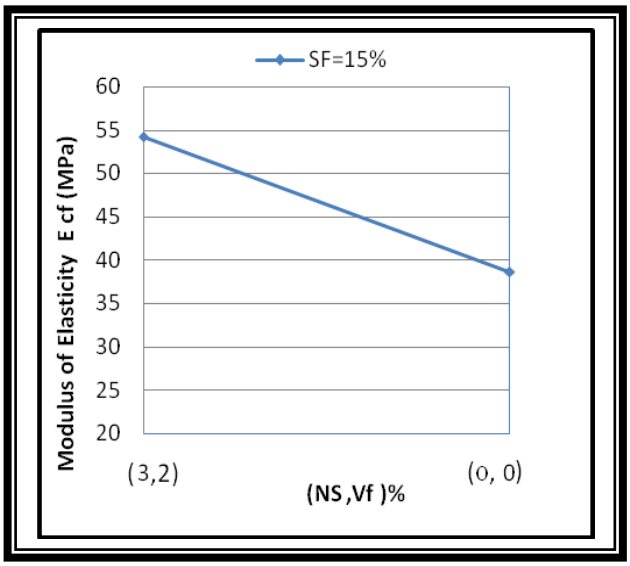

Fig. 4.16: Effect of Dual Absence of Nanosilica and Steel Fibers on Modulus of Elasticity

4.3 Effects of "Material" and "Beam" Parameters on the Structural Performance and Shear Capacity of NSRPC Beams.

The results of the experimental tests carried out on sixteen NSRPC beams in this research are summarized in Table 4.5 , where V_{cr} is the shear force at first observed diagonal shear crack and V_u is the ultimate shear capacity of the tested beam.

The diagonal cracking shear force V_{cr} was considered as that causing the first visible diagonal crack to form within the shear span at mid – depth of the beam and which eventually lead to failure. Since the recording of V_{cr} is usually sensitive to the adjustment of the observer, it cannot be considered as very accurate.

The effects of the following parameters on the shear behaviour of NSRPC beams are to be discussed in this section.

1. Material parameters: Including percentages of nanosilica (NS), silica fume (SF), steel fibers (V_f) and dual absence of (NS) and (V_f).
2. Beam parameters : Including ratio of longitudinal steel bars (ρ), shear span to effective depth ratio (a/d) and presence of steel stirrups.

4.3.1. Effects of Material Parameters on V_{cr} and V_u

The effects of varying the percentages of nanosilica (NS), silica fume (SF), steel fibers (V_f) and the dual absence of (NS) and (V_f) on the diagonal cracking shear force V_{cr} and ultimate shear capacity V_u of the tested NSRPC beams of the present study are shown in Table 4.6 and Figures 4.17, 4-18, 4-19and4-20respectively. .

Table 4.5: Shear Strength Characteristics of the Tested NSRPC Beams

Group No.	Beam	NS %	SF%	Vf%	ρ	a/d	stirrups	f'_{cf} (MPa)	Shear Strength		$\frac{V_u \text{ test}}{V_{cr} \text{ test}}$	Mode of Failure
									Diagonal Cracking V_{cr}(kN)	Ultimate Vu(kN)		
1 Changing NS	B_1	0	15	2	0.0742	3.5	-	120	35	107.5	3.07	DT*
	B_2	1	15	2	0.0742	3.5	-	138.3	42.5	122.5	2.88	DT
	B_3	2	15	2	0.0742	3.5	-	152	45	127.5	2.83	DT
	B_4	3	15	2	0.0742	3.5	-	157.6	47.5	134.5	2.83	DT
2 Changing SF	B_5	3	5	2	00.742	3.5	-	140.6	40	121.5	3.04	DT
	B_6	3	10	2	0.0742	3.5	-	148.7	42.5	126.5	2.98	DT
	B_4	3	15	2	0.0742	3.5	-	157.6	47.5	134.5	2.83	DT
3 Changing V_f	B_7	3	15	0	0.0742	3.5	-	98	27.5	45	1.64	DT
	B_8	3	15	1	00.742	3.5	-	128	40	92.5	2.31	DT
	B_4	3	15	2	0.0742	3.5	-	157.6	47.5	134.5	2.83	DT
4 Changing ρ	B_4	3	15	2	0.0742	3.5	-	157.6	47.5	134.5	2.83	DT
	B_9	3	15	2	0.0857	3.5	-	157.6	57.5	156	2.71	DT
	B_{10}	3	15	2	0.0911	3.5	-	157.6	60	164	2.73	DT
5 Changing a/d	B_4	3	15	2	00.742	3.5	-	157.6	47.5	134.5	2.83	DT
	B_{11}	3	15	2	0.0742	3	-	157.6	52.5	167.5	3.19	DT
	B_{12}	3	15	2	0.0742	2.5	-	157.6	55	208	3.78	DT
	B8	3	15	1	00.742	3.5	-	128	40	92.5	2.31	DT
	B_{13}	3	15	1	0.0742	3	-	128	42.5	109	2.56	DT
	B_{14}	3	15	1	0.0742	2.5	-	128	45	137.5	3.06	DT
6 Presence of Steel Stirrups	B7	3	15	0	00.742	3.5	-	98	27.5	45	1.64	DT
	B15	3	15	0	0.0742	3.5	ϕ6@85	98	30	87.5	2.92	DT
7 Dual Absence of NS and Vf	B4	3	15	2	0.0742	3.5	-	157.6	47.5	134.5	2.83	DT
	B16	0	15	0	0.0742	3.5	-	75	25	35	1.40	DT

- D.T=Diagonal-Tension-Failure

Table 4.6: Effect of Material Parameters on the Shear Capacity of NSRPC Beams

Group No.	Beam	Variable Material Parameter	Other Constant Parameters	Diagonal Crack Shear Force V_{cr} (kN)		Ultimate Shear Capacity V_u (kN)	
				Value	**%Increase**	**Value**	**%Increase**
1 Changing NS	B1 reference	NS=0%	SF=15% V_f=2% ρ=0.0742 a/d=3.5 Stirrups=Nil	35	-	107.5	-
	B2	NS=1%		42.5	21.4	122.5	14
	B3	NS=2%		45	28.6	127.5	18.6
	B4	NS=3%		47.5	35.7	134.5	25.1
2 Changing SF	B5 reference	SF=5%	NS=3% V_f=2% ρ=0.0742 a/d=3.5 Stirrups=Nil	40	-	121.5	-
	B6	SF=10%		42.5	6.3	126.5	4.1
	B4	SF=15%		47.5	18.8	134.5	10.7
3 Changing V_f	B7 reference	V_f=0%	NS=3% SF=15% ρ=0.0742 a/d=3.5 Stirrups=Nil	27.5	-	45	-
	B8	V_f=1%		40	45.5	92.5	105.6
	B4	V_f=2%		47.5	72.7	134.5	198.9
7 Dual Absence of NS and V_f	B4 reference	NS=3% V_f=2%	SF=15% ρ=0.0742 a/d=3.5 Stirrups=Nil	47.5	-	134.5	-
	B16	NS=0% V_f=0%		25	-47.4 decrease	35	-74 decrease

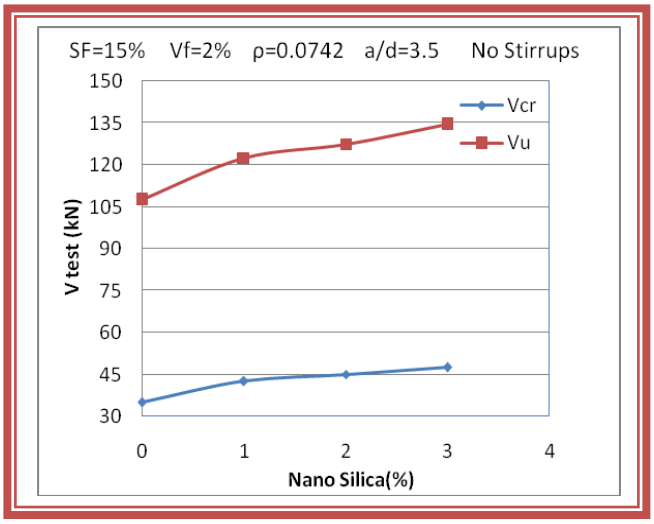

Fig. 4-17 : Effect of Varying Percentage of Nanosilica on Shear Strength of NSRPC Beams

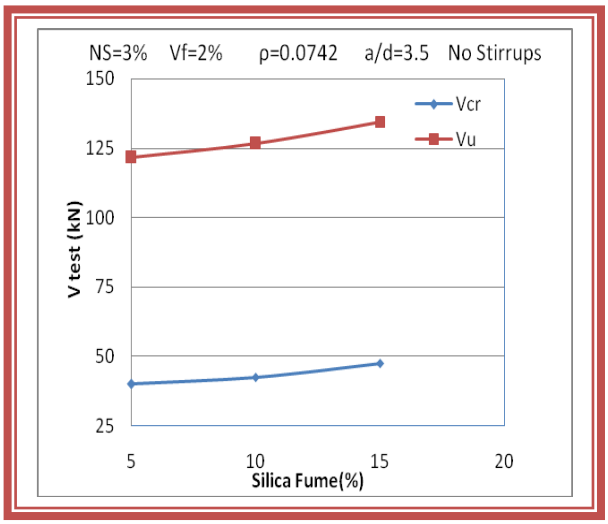

Fig. 4-18:Effect of Varying Percentage of Silica Fume on Shear Strength of NSRPC Beams

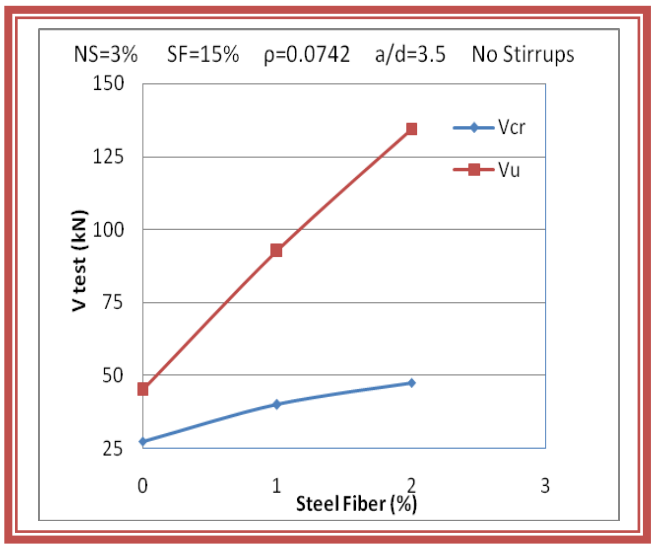

Fig. 4.19: Effect of Varying Percentage of Steel Fibers on Shear Strength of NSRPC Beams

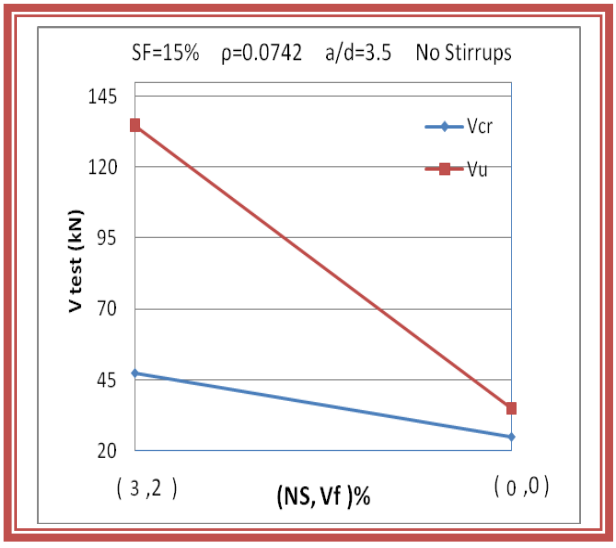

Fig. 4.20: Effect of Dual Absence of Nanosilica and Steel Fibers on Shear Strength of NSRPC Beams

4.3.1.1. Effect of Nanosilica (Group 1)

Table 4.6 and Fig. 4.17 show that by increasing the percentage of nanosilica from 0% in beam B1 to 1% in B2, 2% in B3 and 3% in B4, the diagonal cracking shear force V_{cr} increased from 35kN to 42.5 kN, 45kN and 47.5kN respectively representing a consecutive increase of 21.4%, 28.6% and 35.7% compared with the reference beam B1. The corresponding ultimate shear capacity V_u in these beams also increased from 107.5 kN (B1) to 122.5 kN (B2), 127.5 kN (B3) and 134.5 kN (B4) representing a consecutive increase of 14%, 18.6% and 25.1% compared with B1.

The percentage increases in V_u due to increasing NS are slightly higher than the corresponding percentage increases in V_{cr} and such increases are expected since the use of nanosilica in the concrete mixes reduces the voids between the matrix particles and act as a binder to them which enable the critical shear section to withstand greater shear force. When the section cracks, the zone of the section beyond the crack tip is usually undergoing compression from bending and this also shares in enhancing the shear capacity due to the increased friction between the matrix particles.

4.3.1.2 Effect of Silica Fume (Group 2)

Table 4.6 and Fig. 4.18 show that by increasing the percentage of silica fume from 5% in beam B5 to 10% in B6 and 15% in B4 the diagonal cracking shear force V_{cr} increased from 40kN to 42.5kN and 47.5kN respectively representing a consecutive increase of 6.3% and 18.8% compared with the reference beam B5. The corresponding ultimate shear capacity V_u in these beams also increased from 121.5kN (B5) to 126.5 kN (B6) and 134.5kN (B4) representing respectively an increase of 4.1% and 10.7% compared to B5.

These results clearly indicate that the role of silica fume in enhancing the shear capacity of NSRPC beams is not as strong as that of nanosilica . Despite this minor effect, the use of silica fume in NSRPC is still beneficial in filling the micro voids between cement grains and generating calcium silicate hydrate which both make the concrete matrix richer and denser.

4.3.1.3 Effect of Steel Fibers (Group 3)

The nonfibrous beam B7 is the reference beam and it is used to compare the shear cracking and ultimate shear strengths of the two fibrous NSRPC beams B8 (V_f=1%) and B4 (V_f=2%). In the control "nonfibrous" beam B7, the diagonal cracks appeared directly in the shear span at V_{cr}=27.5 kN and then a sudden and violent complete shear failure occurred shortly after formation of the diagonal crack at ultimate shear force V_u=45kN. The diagonal cracking shear force (V_{cr}) in the nonfibrous NSRPC beam B7 represents 61.1% of the ultimate shear capacity (V_u). Such cracking and failure actually impede the performance of the three shear transfer mechanisms, which are (a) shear stress in the uncracked compression zone (b) friction or interface shear along the diagonal crack surface and (c) dowel action.

With the addition of steel fibers both the diagonal cracking and ultimate shear forces increased, as shown in Table 4.6 and Fig. 4.19.

However, the increase in the ultimate shear force (V_u) seemed more regular and significant than that in the diagonal cracking shear force (V_{cr}). In the fibrous NSRPC beams B8 and B4 where fibers existed at volume fraction (V_f) of 1% and 2% respectively, there was a distinct and stable diagonal cracking load, which was followed by a considerable post- cracking load capacity before attaining the complete failure. Such shear force was of a gradual nature and a number of fine cracks formed. The ratio V_u/V_{cr} seems to increase substantially with increasing V_f. This increasing result is due to the presence of steel fibers which greatly increases the overall rigidity of the beam and

allows NSRPC beams to behave plastically at the onset of shear failure with steel fibers pull out of the cement matrix rather than snap. The essential improvement in the post –cracking shear capacity of fibrous NSRPC beams actually permitted an ample warning with a considerable amount of safety before the complete shear failure became eminent.

Table 4.6 and Fig. 4.19 show that by increasing the percentage of steel fibers from 0% in B7 to 1% in B8 and 2% in B4 the diagonal cracking shear force V_{cr} increased from 27.5kN to 40kN and 47.5kN respectively representing an increase of 45.5% and 72.7% compared with the control nonfibrous NSRPC beam B7. Also for the same increase in the percentage of steel fibers, the ultimate shear strength V_u increased from 45kN for B7 to 92.5kN for B8 and 134.5kN for B4 representing an increase of 105.6 % and 198.9% respectively . This is attributable to two reasons as follows: the first is that the orientation of fibers across the initiating flexural cracks restricted their propagation and transmitted the tensile stresses uniformly to the concrete media surrounding the crack instead of being concentrated at its tip. This would result in reduced stress intensity at the crack tip so that the beam could accommodate an additional load before the initiating flexural crack being transformed into diagonal crack. The second reason is that the steel fibers enhance the performance of the two shear mechanisms (the shear stress in the uncracked compression zone and the interface shear along the diagonal crack surface). This is mainly due to the existence of fibers across the diagonal crack, which restricts the crack propagation through the shear span and tends to tie up the crack opposite sides towards each other. In this manner the shear transfer by the two above mechanisms was further maintained.

In addition, such condition brought about a new additional "fiber shear transfer mechanism" which was not found in nonfibrous beams. A part of the shear force was transferred by this mechanism through the effectiveness of the steel fibers in carrying such a load and transferring it to the surrounding

NSRPC matrix. Therefore, several diagonal cracks were observed in all fibrous beams with relatively high percentage of fibers, thus indicating the redistribution of stresses until the complete pullout of all fibers took place at one critical crack.

4.3.1.4 Effect of the Dual Absence of Nanosilica and Steel Fibers (Group 7).

It has already been shown that the use of optimum dosages of nanosilica and steel fibers in manufacturing a NSRPC beam resulted in a highly efficient shear performance of the beam. Therefore it is thought useful to investigate the percentage reduction in such shear performance when the two mentioned material parameters (NS and V_f) are absent from the concrete mix at the same time.

For this purpose beam B16 was constructed having NS=0% and V_f =0% with the other parameters constant as listed in Table 4.6. The results of tests of this beam were compared with the corresponding results of the reference beam B4 (having NS= 3%, V_f=2% and identical values of the remaining constant parameters). As shown in Table 4.6 and Fig. 4.20, the diagonal cracking shear force was reduced by 47.4%(from 47.5kN for B4 to 25kN for B16) while the ultimate shear capacity was reduced by 74% (from 134.5 kN to 35kN).

It is also of interest to point out that when only the steel fibers was eliminated from the mix the ultimate shear capacity (V_u) was reduced to one-third whereas when both nanosilica of steel fibers were eliminated from the mix V_u was reduced to one-quarter **.**

4.3.2 Effects of Beam Parameters on V_{cr} and V_u

The effect of varying the longitudinal steel reinforcement ratio (ρ), shear span to effective depth ratio (a/d) and the presence of steel stirrups, on the diagonal cracking shear force V_{cr} and ultimate shear capacity V_u of the

tested NSRPC beams of the present research are shown in Table 4.7 and Figs 4.21,(4.22A and B) and 4.23 respectively.

Table 4.7: Effects of Beam Parameters on the Shear Capacity of NSRPC Beams

Group No.	Beam	Variable Beam Parameter	Other constant parameters	Diagonal cracking shear force V_{cr} (kN)		Ultimate shear capacity Vu(kN)	
				Value	%Increases	Value	%Increases
4 Changing ρ	B4 (Reference)	ρ=0.0742	NS=3% SF=15% V_f=2% a/d=3.5 Stirrups= Nil	47.5	-	134.5	-
	B9	ρ=0.0857		57.5	21.1	156	16
	B10	ρ=0.0911		60	26.3	164	21.9
5 changing a/d	B4 (Reference)	a/d=3.5	NS=3% SF=15% Vf=2% ρ=0.0742 Stirrups=Nil	47.5	-	134.5	-
	B11	a/d=3		52.5	10.5	167.5	24.5
	B12	a/d=2.5		55	15.8	208	54.6
	B8 (Reference)	a/d=3.5	NS=3% SF=15% V_f=1% ρ=0.0742 Stirrups=Nil	40	-	92.5	-
	B13	a/d=3		42.5	6.3	109	17.8
	B14	a/d=2.5		45	12.5	137.5	48.6
6 Presence of steel stirrups	B7 (reference)	No Stirrups	NS=3% SF=15% V_f=0 ρ=0.0742 a/d=3.5	27.5	-	45	-
	B15	Stirrups ϕ6@85		30	9.1	87.5	94.4

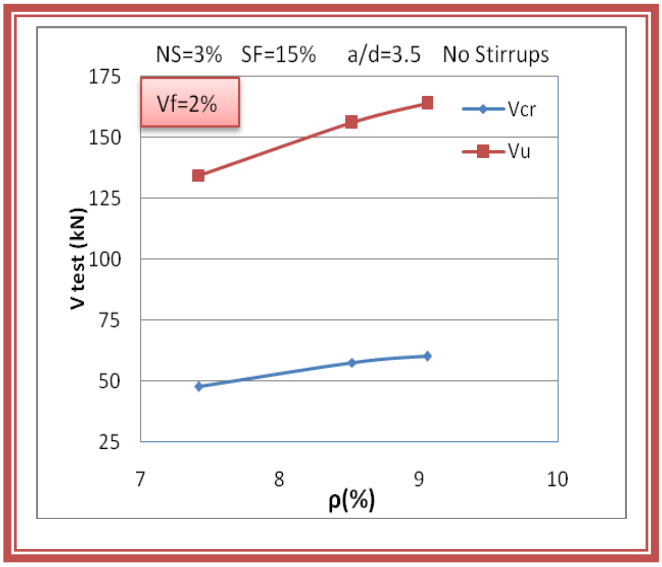

Fig. 4.21: Effect of Varying the Longitudinal Steel Reinforcement Ratio (ρ) on Shear Strength of NSRPC Beams

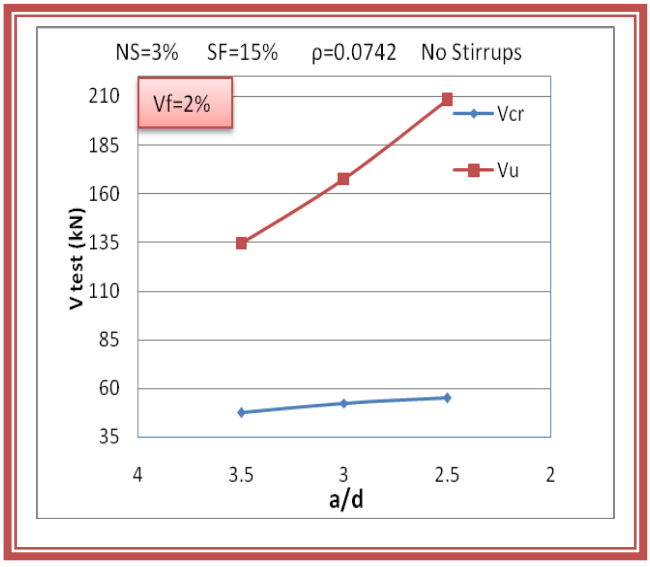

Fig. 4.22A: Effect of Varying the Shear Span to Effective Depth Ratio (a/d) on Shear Strength of NSRPC Beams(the case V_f=2%)

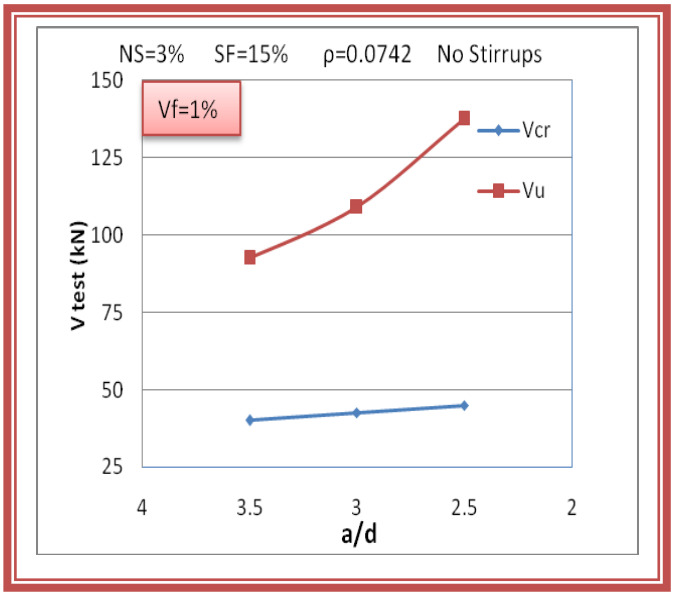

Fig. 4.22B: Effect of Varying the Shear Span to Effective Depth Ratio (a/d) on Shear Strength of NSRPC Beams(the case V_f=1%)

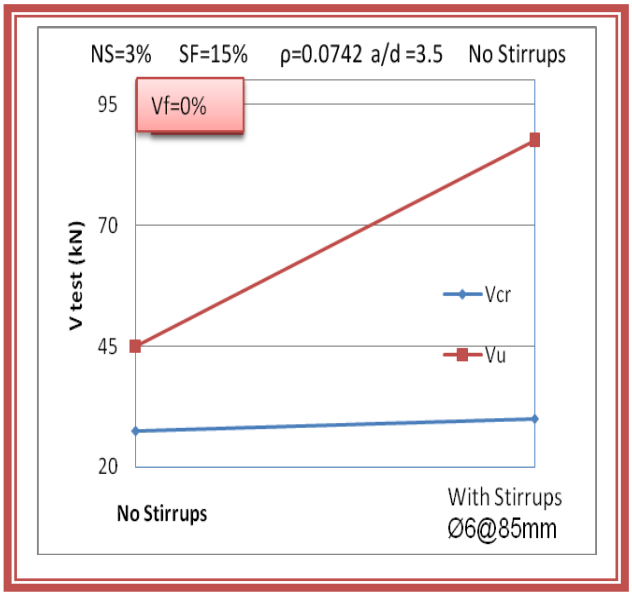

Fig. 4.23: Effect of Varying the Presence of Steel Stirrups (Ø6@85mm) on Shear Strength of Nonfibrous NSRPC Beams

4.3.2.1 Effect of the Longitudinal Steel Reinforcement Ratio ρ(Group 4)

Table 4.7 and Fig. 4.21 show that by increasing the longitudinal steel reinforcement ratio ρ from 0.0742 in beam B4 to 0.0857 in B9 and 0.0911 in B10, the diagonal cracking shear force V_{cr} increased from 47.5 kN to 57.5 kN and 60kN respectively representing a consecutive increase of 21.1% and 26.3% compared with the reference beam B4. The corresponding ultimate shear capacity V_u also increased from 134.5 kN (B4) to 156 kN (B9) and 164 kN (B10) representing a consecutive increase of 16% and 21.9% compared with B4.

The increase in the shear strength of NSRPC beams caused by increasing the steel reinforcement ratio (ρ) can to attributed to the following two main reasons:

1. Increasing ρ leads to slower growth of flexural cracks accompanied by small induced principal stresses for a given applied load and consequently greater shear force to cause diagonal tension crack to form.
2. Increasing ρ increases the dowel action and this leads to formation of shear cracks with a narrower width. Since the friction or interface shear along the diagonal creak surface depends on the crack width, an increase in the friction or interface shear force along the diagonal crack surface is to be expected with an increase in ρ.

4.3.2.2 Effect of the Shear Span to Effective Depth Ratio a/d (Group 5)

The effect of a/d on the shear strength of the tested NSRPC beam is shown listed under group 5 in Table 4.7 and plotted graphically in Figs. 4.22A for the case V_f= 2% and Fig. 4.22B for the case V_f= 1%. It can be seen that generally higher shear strengths V_{cr} and V_u were obtained for lower value of a/d.

For the case V_f=2%, three ratios of a/d were considered; namely a/d=3.5,3 and 2.5 for beam B4 , the reference beam, B11andB12 respectively.

In these beams the diagonal cracking shear force V_{cr} increased from 47.5 kN for B4 to 52.5 kN for B11 and 55 kN for B12 representing a consecutive increase of 10.5% and 15.8%. The corresponding ultimate shear capacity V_u in these beams also increased from 134.5 kN (for B4) to 167.5 kN (for B11) and 208kN (for B12) representing a consequative increase of 24.5% and 54.6%.

For the case V_f= 1%, three beams were constructed; B8 the reference beam with a/d= 3.5, B13 with a/d=3 and B14 with a/d=2.5. The shear force V_{cr} increased from 40kN (for B8) to 42.5 kN (for B13) and 45 kN (for B14) representing a consecutive increase of 6.3% and 12.5%, V_u on the other hand increased from 92.5 kN (for B8) to 109 kN (for B13) and 137.5 kN (for B14) representing a consecutive increases of 17.8% and 48.6%.

The increase in V_u with decreasing a/d is more pronounced than the increase in V_{cr}. The effect of rising shear strength with smaller a/d ratio can be explained so follows: for the same applied load level, any decrease in a/d ratio, means smaller bending moment in the shear span and therefore smaller flexural tensile stress and lesser depth of penetration of flexural crack. This usually requires a higher shear force to initiate a diagonal tensile crack which is usually associated with smaller principal stress.

4.3.2.3 Effect of the Presence of Steel Stirrups (Group 6)

The effect of the presence of steel stirrups on the shear capacity is thought to be best examined considering non- fibrous NSRPC beams. This was followed to eliminate any interference of enhancement in shear strength created by the presence of steel fibers.

For this purpose two typical NSRPC beams having V_f=0 were selected; namely, beam B7 which had no steel stirrups and beam B15 which had 6 mm diameter steel stirrups spaced at 85 mm c/c within its left and right shear spans. As shown listed in Table 4.7 and plotted graphically in Fig.4.23 the diagonal cracking shear force V_{cr} increased from 27.5kN forB7 to 30kN for B15 representing an increase of 9.1% while the ultimate shear capacity V_u

increased from 45 kN for B7 to 87.5 kN (for B15) representing a considerable increase as high as 94.4%.

It is clearly evident from such comparisons that steel stirrups has minor contribution to shear resistance before a shear crack is developed.

However, as a diagonal tension crack forms the steel stirrups will greatly share in resisting higher shear forces until complete shear failure takes place at the onset of yielding and then cut of the steel stirrups.

4.4 Crack Patterns and Failure Mechanisms

Plates 4.1 to 4.7 show the crack patterns of all the tested NSRPC beams arranged respectively according to their classified groups.

From these crack patterns, the following facts can be drawn:

1. All the tested NSRPC beams failed in shear by diagonal tension failure.
2. Failure of all beams resulted from tensile fracture across a single dominant diagonal crack or from a coalescence of inclined cracks that led to the formation of a dominant diagonal crack.
3. The failure mechanism was seen to depend largely on two main parameters, one is the material parameter V_f (steel fibers volumetric percentage) and the other is the beam parameter a/d (shear span to effective depth ratio).
4. Nonfibrous NSRPC beams were seen to fail shortly after the formation of the critical diagonal crack, whereas multiple cracks were seen to form (after initial cracking) in fibrous NSRPC beams. The quantity of fibers was found to have a significant influence on the rate of growth of these cracks and their widths. In beams with lower percentage of steel fibers, a faster rate of crack growth with larger crack width were recorded. In contrast, slowly growing fine cracks were seen to form in beams with higher percentage of steel fibers.
5. The cracking and ultimate loads were higher in beams with higher V_f than beams with lower V_f. When V_f increased from 0% (beam B7) to 1%(B8) and 2% (B4), P_{cr} increased by 45.5% and 72.7% respectively while P_u increased by 105.6% and 198.9% respectively.

6. The ultimate loads were seen to be much higher than the inclined cracking loads in beams with higher percentage of steel fibers V_f than in beams with lower or without V_f (i.e nonfibrous beams). For a constant ratio a/d=3.5, the ratio P_u/p_{cr} ranged from 2.83(beam B4, V_f= 2%) to 2.31 (beam B8, V_f=1%) to 1.64(beam B7, V_f=0%) .
7. Three ratios of a/d namely 3.5,3 and 2.5were chosen to test the NSRPC beams. Within these ratios, NSRPC beams failed in shear. But if a higher a/d ratio had been chosen, well beyond 3.5, the beam would have failed by flexural failure mechanism. Also that if a lower a/d ratio had been chosen, well below 2.5, the beam would have been classified as a deep beam failing by a definite inclined diagonal shear failure.
8. The cracking and ultimate loads were found to be higher in beams with lower a/d ratio than in beams with higher a/d ratio. This is because the bending moment in a beam with lower a/d ratio is relatively small giving a smaller bending stress and hence a lesser principal stress for a given applied load, and consequently the greater must be the shear to cause diagonal tension cracking to form.

The maximum percentages increase in P_{cr} and P_u due to decrease in a/d were found in beams having V_f= 2% as follows:

- Maximum percentage increase in P_{cr} was 15.8%, due to a decrease in a/d from 3.5 (beam B4) to 2.5 (beam B12).
- Maximum percentage increase in P_u was 54.6%, due to a decrease in a/d from 3.5 (beam B4) to 2.5 (beam B12).

9. The ratio P_u/P_{cr} was found to be higher in beams with lower a/d ratio than in beams with higher a/d ratio. The ratio P_u/P_{cr} for the tested NSRPC beams was found to range from a maximum value of 3.78 (for beam B12 having a/d= 2.5 and V_f= 2%) to a minimum value of 2.34 (for beam B8 having a/d= 3.5 and V_f= 1%).

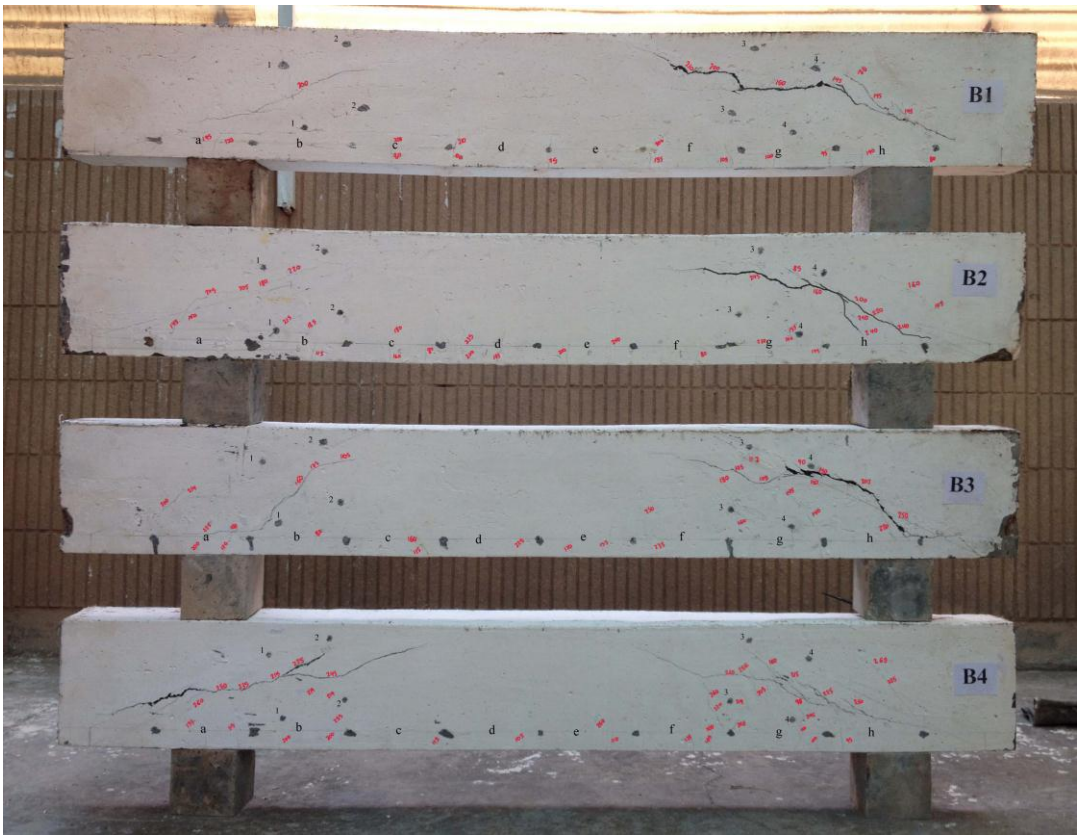

Plate 4.1 Crack Patterns of NSRPC Beams (B1,B2,B3,B4with Varying NS)

Plate 4.2 Crack Patterns of NSRPC Beams (B5,B6,B4 with Varying SF)

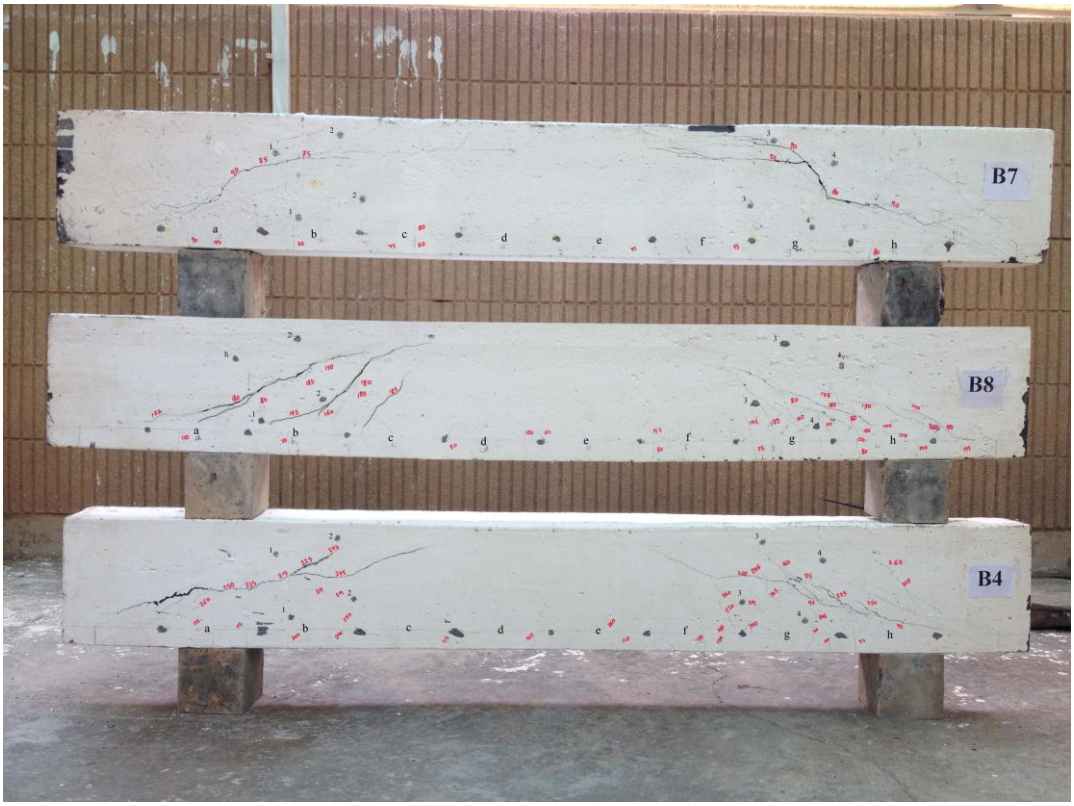

Plate 4.3 Crack Patterns of NSRPC Beams (B7,B8, B4 with Varying V_f)

Plate 4.4 Crack Patterns of NSRPC Beams (B4,B9,B10 with Varying ρ)

Plate 4.5A Crack Patterns of NSRPC Beams (B4,B11,B12 with Varying a/d ,V_f=2%)

Plate 4.5B Crack Patterns of NSRPC Beams (B8,B13,B14with Varying a/d, V_f=1%)

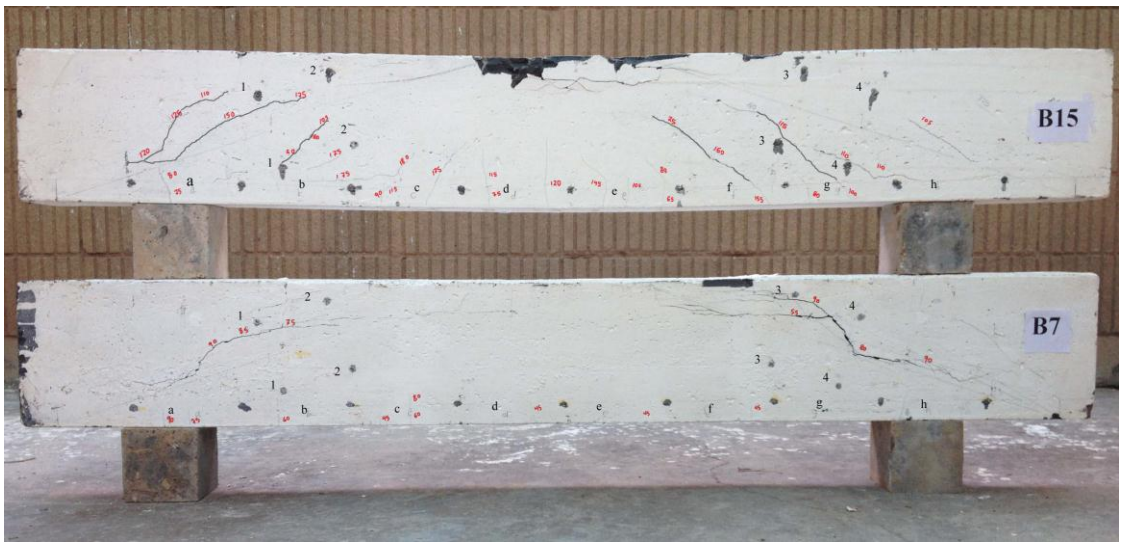

Plate 4.6 Crack Patterns of NSRPC Beams (B7,B15 with Steel Stirrups)

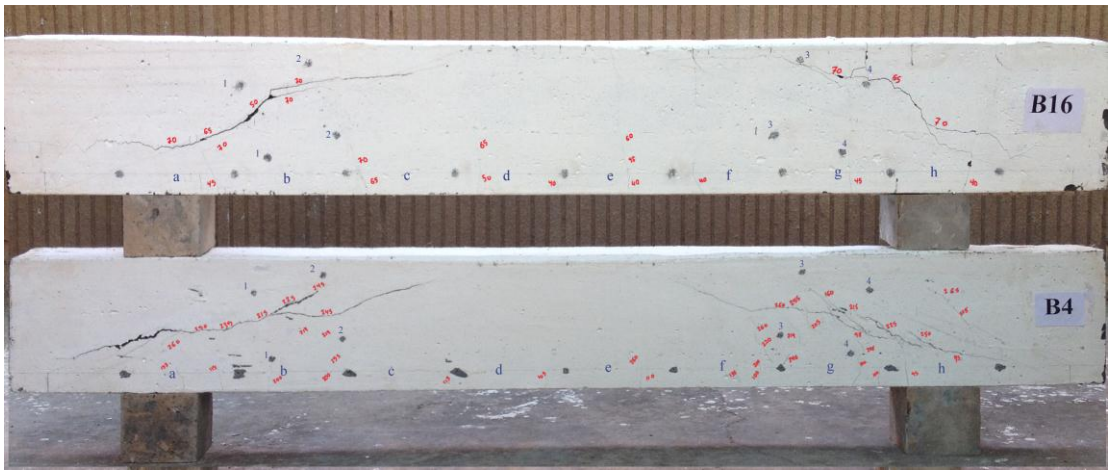

Plate 4.7 Crack Patterns of NSRPC Beams (B4,B16 with Dual Absence of NS and Vf)

4-5 load- Deflection Behaviour

The load- deflection characteristics of the tested sixteen NSRPC beams are listed in Table 4.8. Figures 4.24 to 4.30 show the load-deflection curves of these beams plotted in groups, where the beams of each group had one variable parameter with the values of the remaining parameters kept constant. Deflections for all beams were measured using a dial gage located at mid- span.

The general picture of any of these load- deflection curves indicates that the beam (tested under the action of two transverse point loads) exhibited the following three distinct stages:

1. The first stage is the stage of elastic behaviour in which the flexural stresses are linearly distributed over the beam depth at the central region of the span while the shear stresses are elastically distributed over the beam depth in the two shear spans of the beam. Thus the load- deflection relationship in this stage is linear with constant slope.
2. In the second stage and because of the small a/d ratios used in the beams (a/d= 2.5, 3 and 3.5), the bending moment in the beam was comparatively small compared to the induced shear force in the two shear spans which caused inclined cracks to form there. These cracks developed as the load on the beam was increased resulting in a reduction in the beam stiffness. The load- deflection curve changed characteristics from linearity to non-linearity after showing a small rise in load with increasing deflection then a sharp increase in load. However the slope of the load- deflection curve after diagonal shear crack was formed became smaller.

Table 4.8: Load- Deflection Characteristics of the Tested NSRPC Beams

Beam	Diagonal Cracking Load P_{cr} (kN)	Deflection at First Crack Load Δcr (mm)	Ultimate Load P_u (kN)	Deflection at Ultimate Load Δ_o (mm)	$\frac{P_u}{P_{cr}}$	Ductitiy Ratio Ψ $\Psi=\frac{\Delta_o}{\Delta_{cr}}$
B1	70	3.15	215	14.5	3.07	4.6
B2	85	3.6	245	13.3	2.88	3.7
B3	90	3.5	255	12.7	2.83	3.6
B4	95	3.6	269	12.3	2.83	3.4
B5	80	2.8	243	13.8	3.04	4.9
B6	85	3.0	253	13.2	2.98	4.4
B7	55	3.65	90	5.7	1.64	1.6
B8	80	3.4	185	9.0	2.31	2.6
B9	115	3.7	312	11.5	2.71	3.1
B10	120	3.8	328	10.8	2.73	2.8
B11	105	2.3	335	12.9	3.19	5.6
B12	110	1.5	416	13.4	3.78	8.9
B13	85	2.7	218	10.2	2.56	3.8
B14	90	1.9	275	11.0	3.06	5.8
B15	60	2.8	175	9.2	2.92	3.3
B16	50	4.5	70	6.0	1.40	1.3

3. In the third stage, the beam reached its ultimate strength and failed in shear with the diagonal crack extended towards the point load.

In all the tested NSRPC beams, the mid- span deflection at ultimate load (Δ_o) was recorded immediately after the ultimate load was reached. Beyond the ultimate load, the rate of increase in mid- span deflection was so fast that no stable and reliable deflection reading could be taken. The ductility ratioΨ was calculated as the ratio of mid- span deflection at ultimate load (Δ_o) to the mid-span deflection at the first visible shear crack (Δ_{cr}).

However, nonfibrous NSRPC beams (V_f=0) also showed linear elastic- deflection behaviour at the start of loading which was then changed to nonlinear behaviour after the diagonal crack grew and widened. But shortly after the appearance of the diagonal crack in the shear span, a final shear failure occurred suddenly and violently. Therefore the second and third stages can be described as interference stages in these beams.

Following is a description of the effect of each variable parameter on the load- deflection response:

4.5.1 Effect of Nanosilica (Group 1)

Fig. 4.24 shows the effect of increasing the percentage of Nanosilica (NS) on the load- deflection (P-Δ) relationship of NSRPC beams, with the other parameters kept constant (SF= 15%, V_f= 2%, ρ=0.0742 , a/d= 3.5, without stirrups). These are beams B1(NS= 0%), B2(NS= 1%), B3(NS= 2%) and B4(NS= 3%) which were all classified as group 1.

The following remarks can be drawn from this figure:

1. At any load level, the deflection decreases as the percentage of nanosilica is increased. The slope of P-Δ curve in the initial elastic stage is highest in the beam of highest NS and is reduced as NS decreases. This behaviour may be attributed to the enhanced stiffness of the NSRPC beams and improved

mechanical properties of the concrete such as (modulus of elasticity, modulus of rupture, splitting tensile strength and compressive strength).

2. The deflection (Δ_o) at ultimate load is greater in a beam with lower NS while the ultimate load (P_u) is higher in a beam with higher NS. A comparison of results between beam B4 (NS= 3%) and beam B1 (NS= 0% taken as a reference beam) shows that for beam B4, Δ_o is reduced by 15.2% and P_u is increased by 25.1%.
3. According to the point outlined in the preceding clause, the ductility ratio (Ψ) is reduced by increasing NS. Comparing Ψ of beam B4 with that of beam B1 shows a reduction of 26.1%. It can therefore be concluded that the use of higher percentage of NS makes the beam stronger but more brittle.

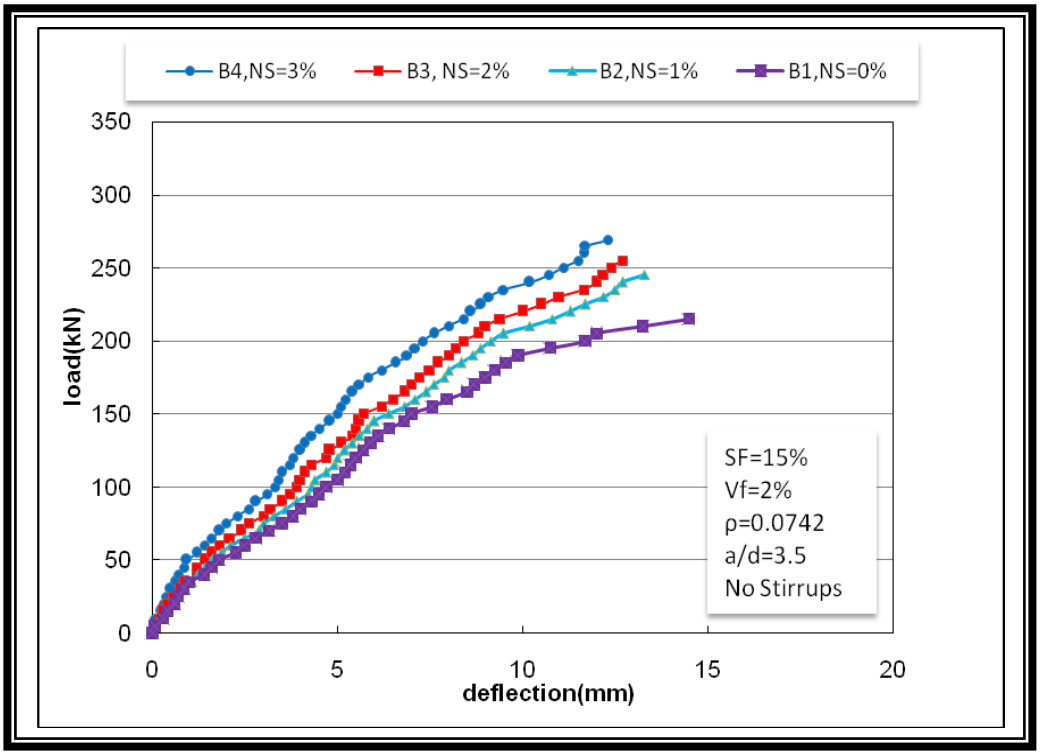

Fig. 4.24: Load–Deflection Curves of NSRPC Beams (B1,B2,B3,B4 -Group 1)

4.5.2 Effect of Silica Fume (Group 2)

Fig 4.25 shows the effect of increasing the percentage of silica fume (SF) on the P-Δ relationship of NSRPC beams with the other parameters kept constant (NS= 3%, V_f= 2%, ρ= 0.0742, a/d= 3.5, no stirrups). These are beams B5 (SF= 5%), B6 (SF= 10%) and B4 (SF= 15%) which were classified as group 2 in Table 4.5.

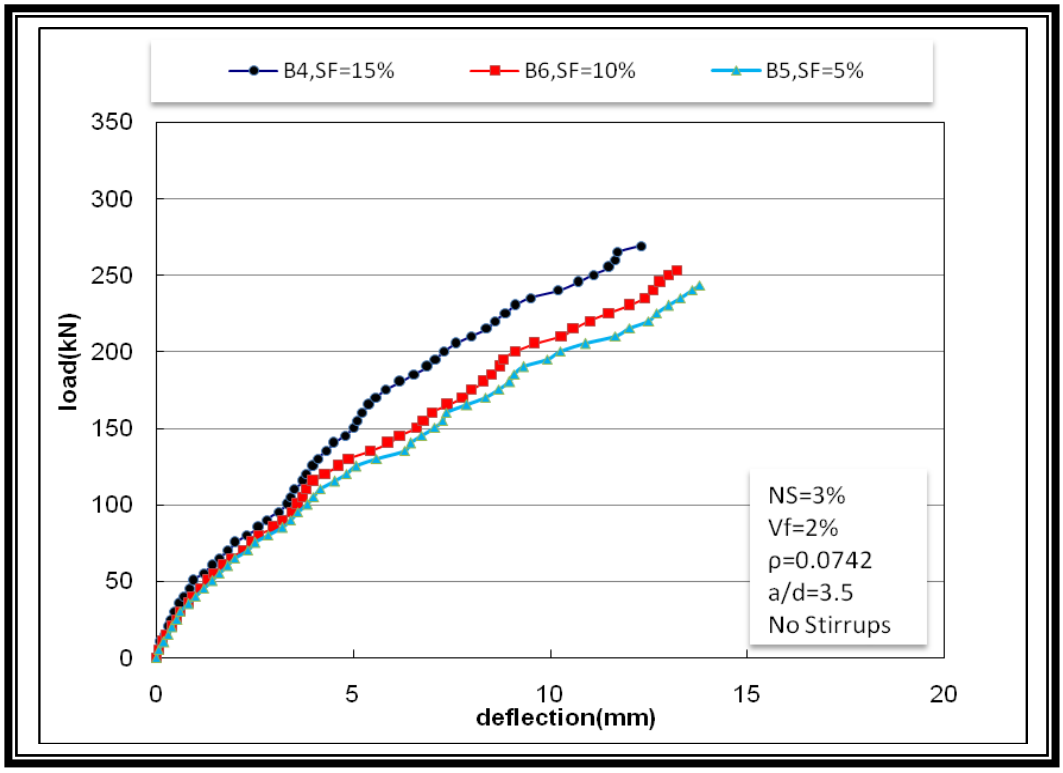

Fig. 4.25: Load–Deflection Curves of NSRPC Beams (B5,B6,B4 -Group 2)

Similar remarks to those stated in the previous article on the effect of nanosilica can be drawn here. With reference to Fig 4.25 these remarks are:

1. For a specific value of load, a smaller deflection was recorded in beam with a higher SF resulting in a steeper P-Δ curve especially at the initial elastic stage. This can be attributed to the enhanced mechanical properties of the concrete containing higher percentages of silica fume.

2. A higher ultimate load (P_u) associated with a lower deflection (Δ_o) was attained in a beam with a higher percentage of SF. Comparison of results between beam B4(SF= 15%) and beam B5(SF= 5% taken as a reference beam) shows that for beam B4, P_u increased by 10.7% while Δ_o decreased by 10.9%.
3. Accordingly the ductility ratio (Ψ) was reduced by increasing SF. A reduction of Ψ as high as 30.6% was obtained when SF was increased from 5% (B5) to 15% (B4).Therefore using higher percentage of silica fume makes the beam stronger but more brittle.

4.5.3 Effect of Steel Fibers (Group 3)

The effect of varying the percentage of steel fibers (V_f) on the load-deflection behaviour of NSRPC beams is shown in Fig. 4.26. Three percentages of V_f were used; V_f= 0% (beam B7 taken as the reference beam), V_f= 1% (B8) and V_f= 2% (B4).

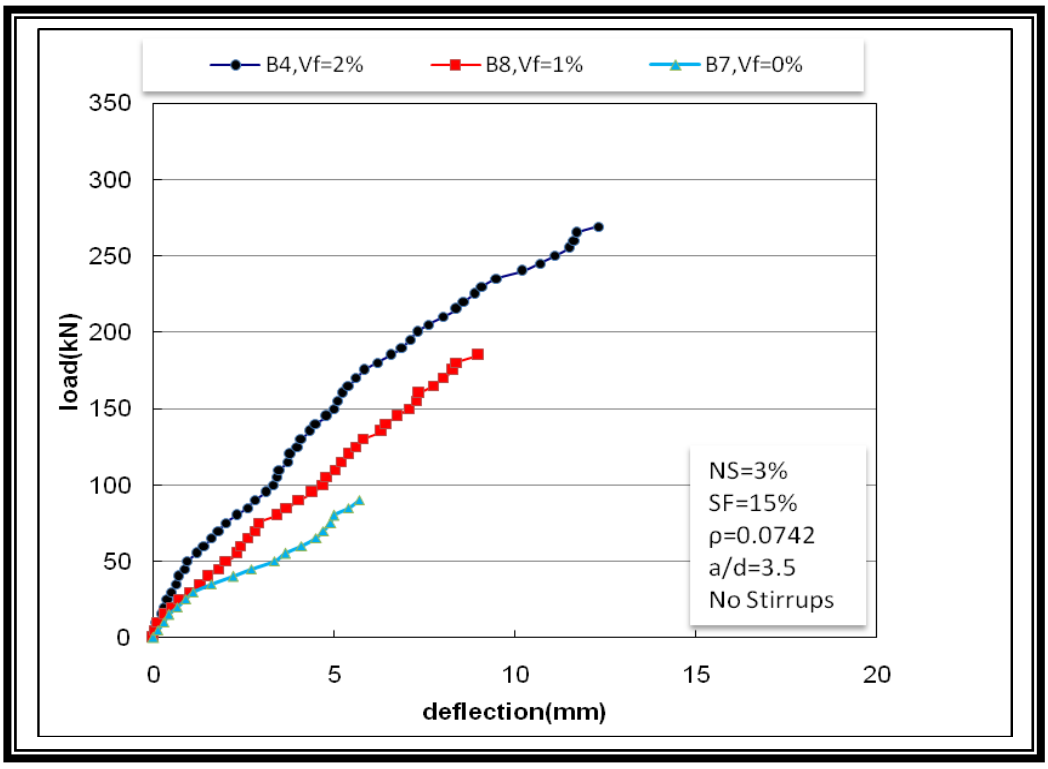

Fig. 4.26: Load–Deflection Curves of NSRPC Beams (B7,B8,B4-Group 3)

In these beams which were classified as group 3, the other parameters were kept constant (NS= 3%, SF= 15%, ρ= 0.0742, a/d= 3.5, no stirrups). It can be seen from Fig. 4.26 and Table 4.8 that:

1. The slope of P-Δ curve was largely increased with increasing V_f and that the P-Δ curve of the nonfibrous beam B7 had the smallest slope. This is expected since the presence of steel fibers in the concrete can greatly enhance its mechanical properties and consequently increase its structural performance.
2. Using higher percentage of steel fibers (V_f) resulted in higher ultimate load (P_u) associated with greater deflection (Δ_o). A comparison of results between the reference beam B7 (V_f= 0%) and beam B4(V_f= 2%) shows that for beam B4, P_u and Δ_o were increased by 198.9% and 115.8% respectively.
3. This very high increases in P_u and Δ_o due to increase in the percentage of steel fibers (V_f) had resulted in an apparent increase in the ductility ratio (Ψ) as well. A percentage increase in Ψ as high as 112.5% was obtained when V_f was increased from 0% (B7) to 2% (B4).Therefore using higher percentage of steel fibers (though should not be greater than 2% to avoid undesirable fibers balling) can make the beam stronger and more ductile. This is normally expected since the steel fibers have the efficiency of arresting the propagation and controlling the growth of the flexure and diagonal cracks within the beam when they are crossed by them, and hence, steel fibers maintain the beam integrity throughout the post-cracking stages of behaviour. The beam, hence, could withstand greater loads and deflection before failure.

4.5.4 Effect of Longitudinal Steel Ratio ρ (Group 4)

The effect of increasing the longitudinal steel ratio (ρ) on the load-deflection behaviour of NSRPC beams is shown in Fig 4-27. Three values of ρ were used; ρ= 0.0742 (beam B4 taken as the reference beam), ρ= 0.0857 (B9) and ρ= 0.0911 (B10).In these beams which were classified as group 4, the other parameters were kept constant (NS= 3%, SF= 15%, V_f= 2%, a/d= 3.5, no stirrups).

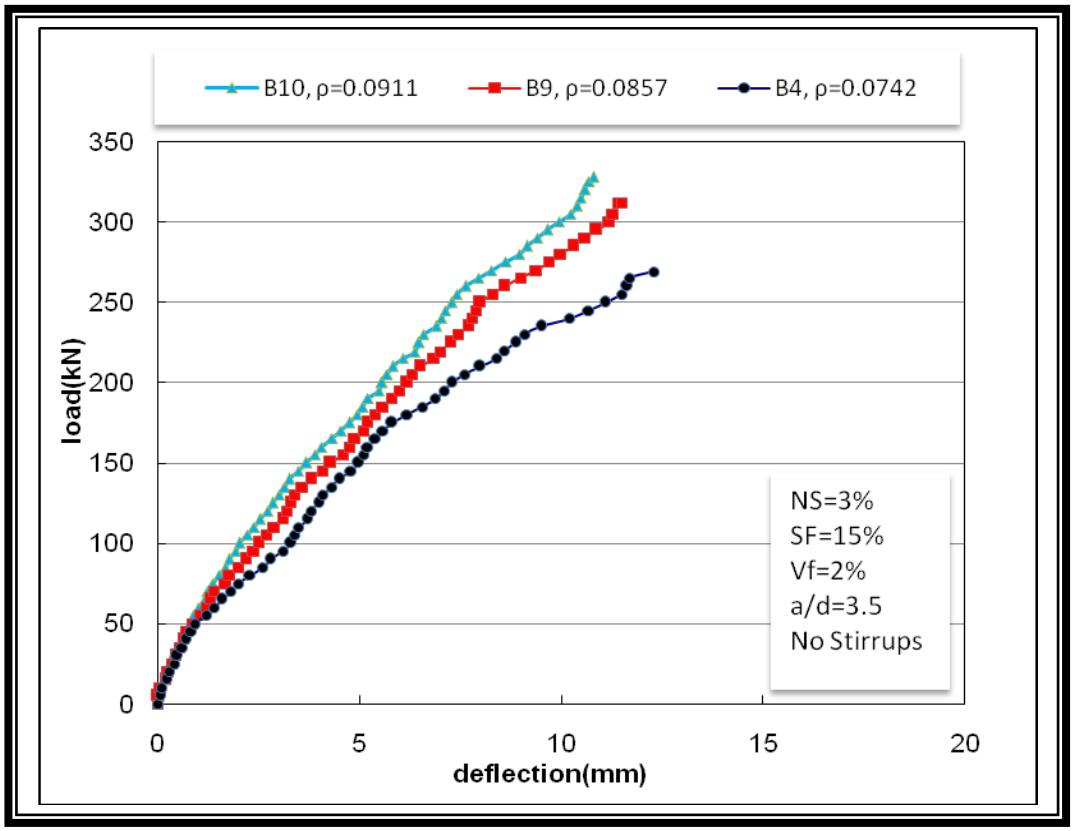

Fig. 4.27: Load–Deflection Curves of NSRPC Beams (B4,B9,B10 -Group 4)

It can be concluded from this figure and Table 4.8 that:

1. The stiffness of the beam (represented by the slope of P-Δ curve) was found higher in the beams with higher ρ especially after shear cracks occurred. This behaviour can be attributed to two facts. One is that the

neutral axis in beams with higher ρ shifts location towards the tension face thus increasing the moment of inertia of the cracked section. The other fact is that a better contribution of dowel action exists in a beam with higher ρ and this helps in increasing the shear strength and delaying the propagation of shear cracks. Therefore the beam with the highest ρ (beam B10) carried greater ultimate load(P_u) associated with slightly lesser deflection (Δ_o) at failure.

2. Comparison of results between the reference beam B4 (ρ= 0.0742) and beam B10 (ρ= 0.0911) shows that for beam B10, P_u was higher by 21.9% while Δ_o was lower by 12.2%.
3. Accordingly the ductility ratio (Ψ) decreased upon increase of ρ. A percentage reduction inΨ of 17.6% was obtained when ρ was increased from 0.0742 (B4) to 0.0911 (B10). Therefore using higher ρ makes the NSRPC beam stiffer but more brittle.

4.5.5 Effect of Shear Span to Effective Depth Ratio a/d (Group 5)

Variation of the shear span to effective depth ratio a/d in the tested NSRPC beams is classified as group 5 in Table 4.5. To show the effect of a/d on the P-Δ behaviour, two cases were considered; namely the case of V_f= 2% and the case of V_f= 1%.

Three ratios of a/d namely 3.5,3 and 2.5 were chosen for either case. In the first case (V_f=2%), the beam B4(a/d= 3.5) was taken as the reference beam and its P-Δ curve was compared with the corresponding curves of beams B11 (a/d= 3) and B12 (a/d= 2.5)shown in Fig. 4.28a. In the second case (V_f= 1%), the beam B8 (a/d= 3.5) was the reference beam whose P-Δ curve was compared with those of beams B13 (a/d= 3) and B14 (a/d= 2.5)shown in Fig. 4.28b.

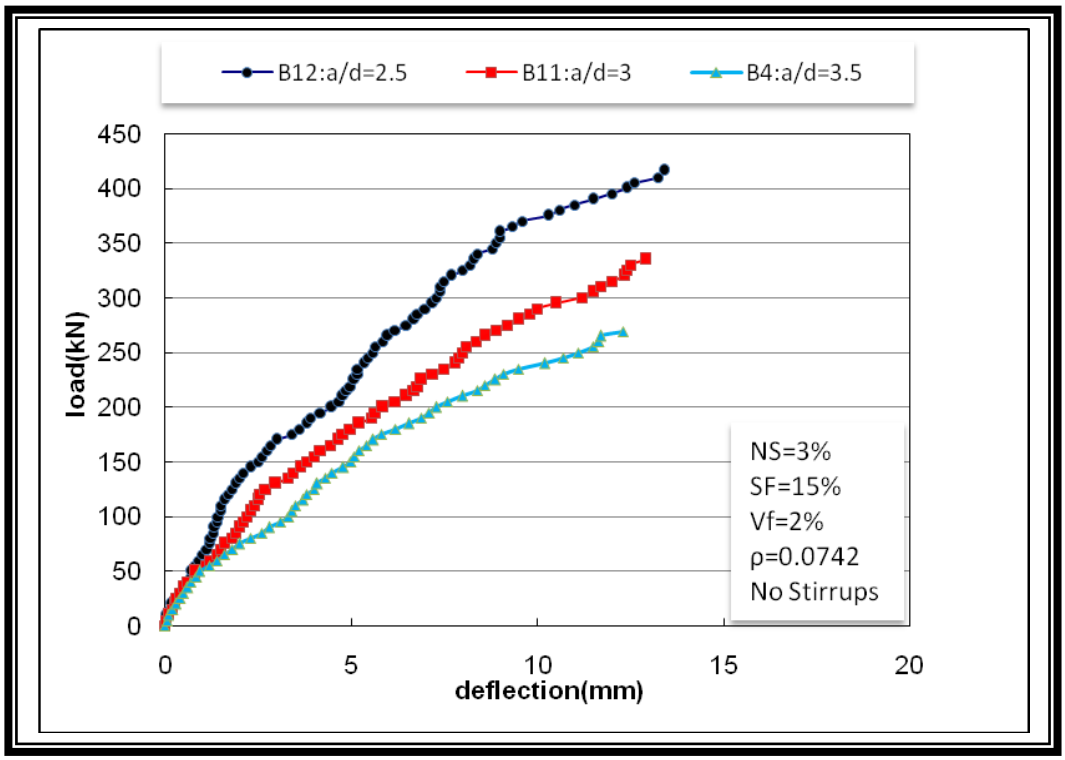

Fig. 4.28a: Load-Deflection Curves of NSRPC Beams (B4,B11,B12 -Group 5,Vf=2%)

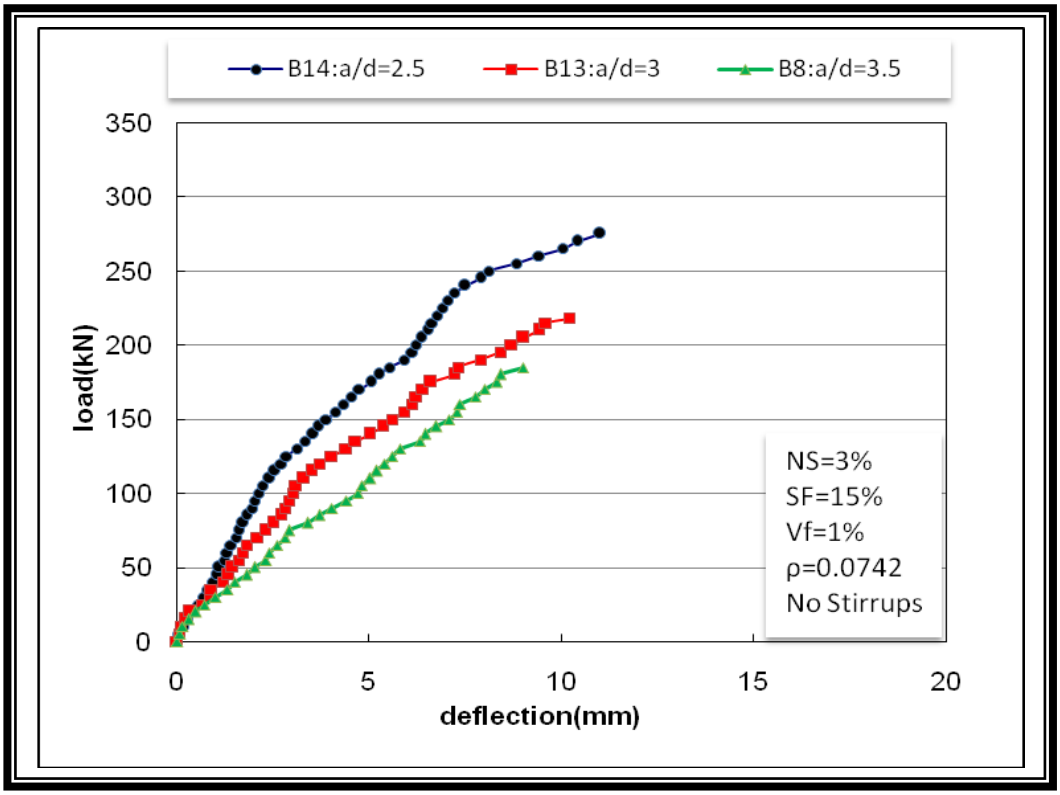

Fig. 4.28b: Load–Deflection Curves of NSRPC Beams (B8,B13,B14 -Group 5,Vf=1%)

The following remarks were drawn from such comparison:

1. The slope of the P-Δ curve was largely increased with decreasing a/d ratio and that beam B12 having the highest V_f (V_f= 2%) and lowest a/d (a/d= 2.5) showed a higher ultimate load (P_u) and associated deflection(Δ_o) than all the other beams. This is because the use of a smaller a/d ratio resulted in a smaller bending moment induced in the beam and this enabled the beam to carry higher ultimate load (P_u) associated with a slightly increased deflection (Δ_o) at failure.
2. Comparison of results (for the case V_f= 2%) between the reference beam B4 (a/d= 3.5) and beam B12 (a/d= 2.5) shows that for beam B12, P_u and Δ_o increased by 54.6% and 8.9% respectively. For the case V_f= 1% the percentage increase in P_u and Δ_o for beam B14 (a/d= 2.5) compared with the reference beam B8 (a/d= 3.5) were 48.6% and 22.2% respectively.
3. The ductility ratio (Ψ) was largely increased by decreasing a/d ratio. For the case V_f= 2%, Ψ increased by 161.8% as a/d decreased from 3.5 (B4) to 2.5 (B12), while for the case V_f= 1%, Ψ increased by 123.1%. Therefore using smaller a/d ratio makes the beam sttiffer and more ductile.

4.5.6 Effect of Presence of Steel Stirrups (Group 6)

Fig 4.29 shows the effect of using steel stirrups (6mm diameter spaced at 85 mm c/c in the two shear spans) on the load- deflection characteristics of NSRPC beams. In this group two beams were considered, beam B7 without stirrups and taken as the reference beam and beam B15 with stirrups.

The other parameters were kept constant in these two beams (NS= 3%, SF= 15%, V_f= 0%, ρ= 0.0742 and a/d= 3.5).

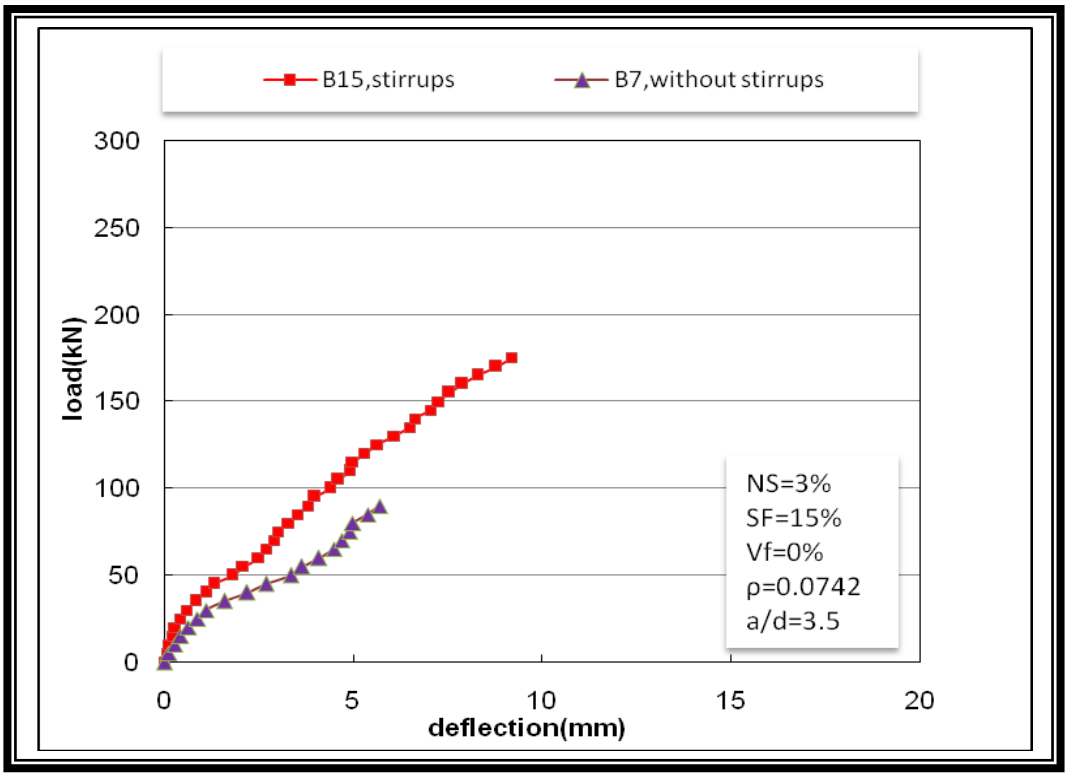

Fig. 4.29: Load–Deflection Curves of NSRPC Beams (B7,B15, -Group 6)

Comparison of the P-Δ curves of these two beams indicate the followings:

1. Beam B15 (with stirrups) showed a steeper P-Δ curve than B7 (without stirrups) indicating that the steel stirrups worked as stiffeners to the beam at all stages of loading including the early elastic stage where the beam was uncracked. It can be argued that the steel stirrups helped in providing a composite section with the uncracked concrete during the elastic uncracked stage and its contribution of shear resistance increased largely after the formation of diagonal shear crack since part at the shear resisting force was carried as tensile forces by these steel stirrups.
2. The use of steel stirrups in beam B15 resulted in higher ultimate load (P_u) associated with greater deflection (Δ_o) than those of beam B7 (without

stirrups). The percentages of increase in P_u and Δ_o were of the order 94.4% and 61.4% respectively.

3. The percentage increase in the ductility ratio (Ψ) resulting from the use of stirrups was of the order 106.3%. It is obvious that using steel stirrups increases the shear capacity of the NSRPC beam and makes it more ductile.

4.5.7 Effect of the Dual Absence of Nanosilica and Steel Fibers (Group 7)

The results of the experimental tests carried out on NSRPC beams in this research assured the efficiency of nanosilica and steel fibers in enhancing the shear capacity of beams as well as increasing their ductility ratio. Therefore a beam with higher NS and V_f is expected to be stiffer and more ductile than a beam free of NS and V_f. The exact effects are studied through group 7 where results of tests of two extreme beams are compared; beam B4 (having NS= 3%, V_f= 2%) and beam B16 (having NS=0% and V_f=0%) as shown in Fig. 4.30. Two other beams having extra combinations of NS and V_f (beam B1, NS= 0%, V_f= 2% and B7, NS= 3% and V_f= 0%) are also included in this group to indicate the intermediate effects. Comparison of the P-Δ curves of these four beams revealed the followings:

1. The highest slope of the four P-Δ curves shown in Fig. 4.30 is that of beam B4 which contained the optimum percentages of NS and V_f (NS= 3%, V_f= 2%). The slopes of the P-Δ curves of the other three beams were found to decrease as NS and / or V_f were absent, and the absence of V_f was found more effective in lowering the slope of the curve (i.e weakening the beam stiffness) than the absence of NS. The weakest beam was found to be B16 which was free of nanosilica and steel fibers.
2. The absence of NS and/ or V_f resulted in lower ultimate loads (P_u) associated with smaller deflections (Δ_o) at failure. The maximum

percentages decrease in P_u and Δ_o were found in beam B16 (NS=0, V_f=0) compared to beam B4 (NS= 3%, V_f= 2%) which were of the order 74% and 51.2% respectively.

3. The ductility ratio (Ψ) was found to decrease largely by the absence of both NS and V_f. A comparison of results between the optimum beam B4 and the nonfibrous- non NS beam B16 showed a percentage reduction in Ψ as large as 161.5%. Therefore a reactive powder concrete beam free of nanosilica and steel fibers can be said to be of extremely weak shear capacity and highly brittle.

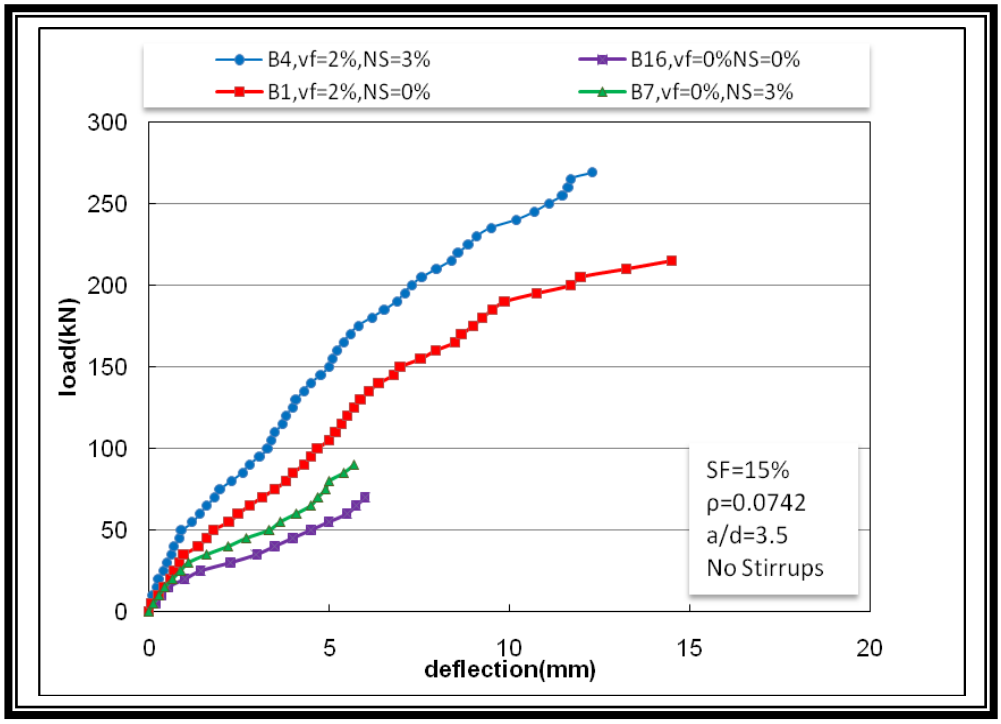

Fig. 4.30: Load–Deflection Curves of NSRPC Beams (B4,B1,B7,B16 -Group 7)

4.6 Load- Maximum Crack Width Relationship

The load- crack width curves for all the tested NSRPC beams are plotted in Figs. 4.31 to 4.37.

Fig. 4.31 shows a comparison among curves belonging to beams B1 (NS= 0%), B2 (NS= 1%), B3 (NS= 2%) and B4(NS= 3%) of group 1. It can be observed from this figure that as nanosilica NS was increased in the beam, a lesser width of shear crack at the onset of shear failure and along all stages of loading was obtained. The reduction in the crack width was due to the decrease in the pores of the concrete matrix when nanosilica was added, which increased the tensile strength of the concrete and arrested the growth of the shear cracks.

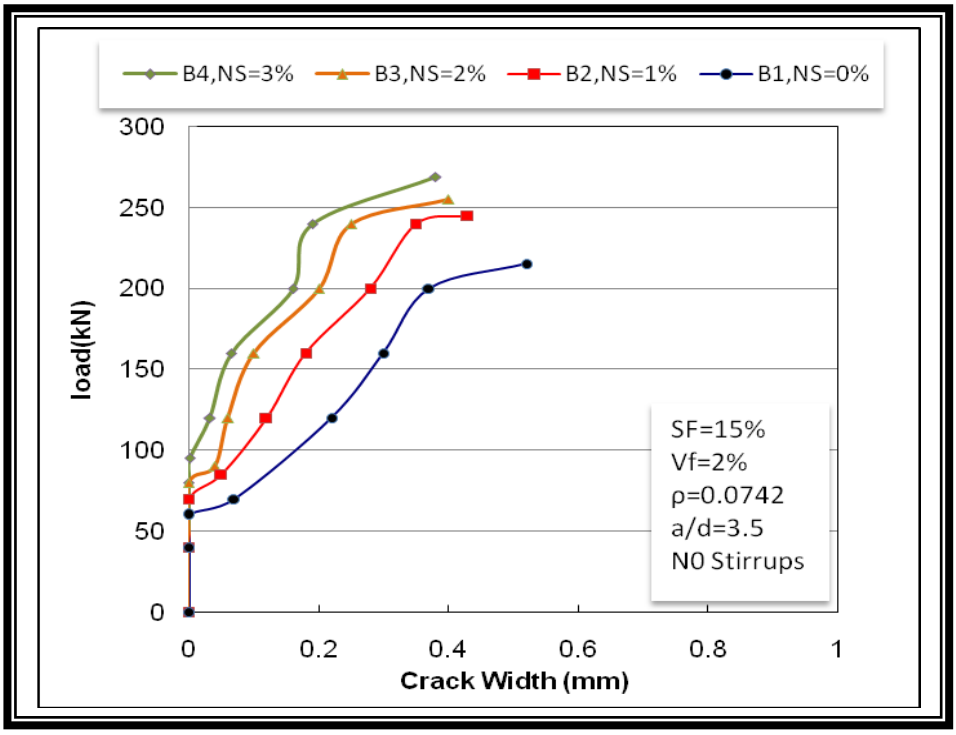

Fig.(4-31): Load-Crack Width Curves of NSRPC Beams (B1,B2,B3,B4-Group 1)

Fig 4.32 shows the effect of increasing silica fume content SF on the maximum crack width for all stages of loading. It can be seen from this figure that with increasing SF the width of the shear crack at failure was lesser. The same reason explained for the effect of NS in the previous paragraph holds true for the effect of SF.

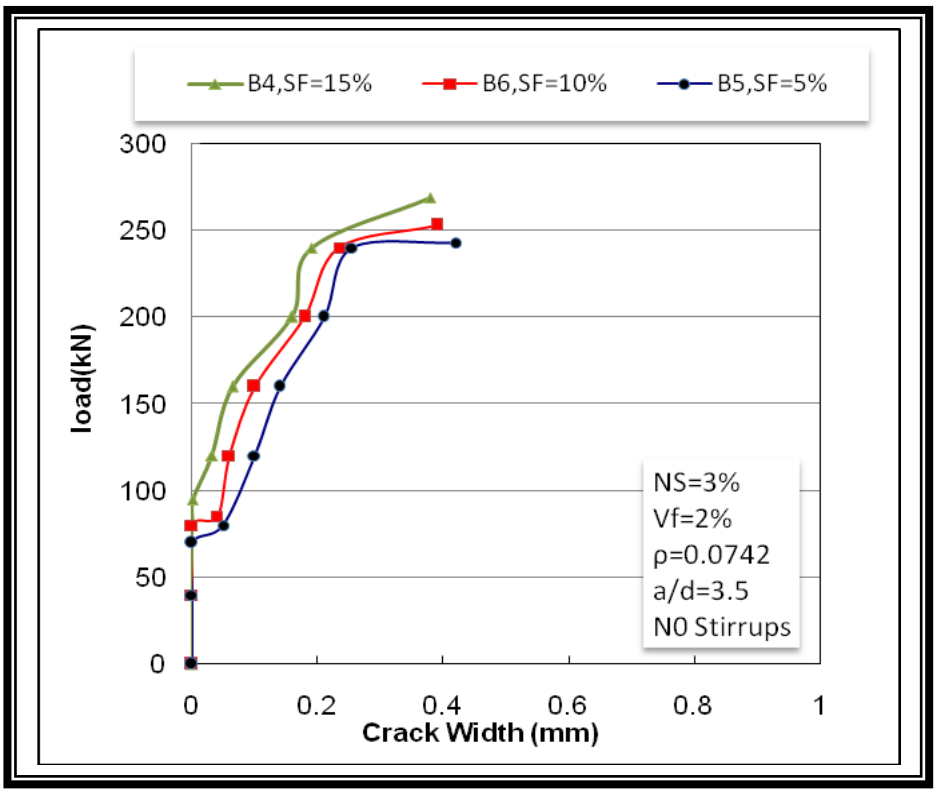

Fig. 4.32: Load-Crack Width Curves- NSRPC Beams (B5,B6,B4-Group 2)

Fig. 4.33 shows the effect of varying the percentage of steel fibers V_f on the maximum crack width for all stages of loading. The figure clearly shows that using higher percentage of steel fibers resulted in lesser shear crack width at the onset of shear failure and at all can be stages of loading. The reduction in crack width can be attributed to the increase in the bond strength between the steel fibers and the concrete matrix which arrested the growth of shear cracks and delayed the shear failure.

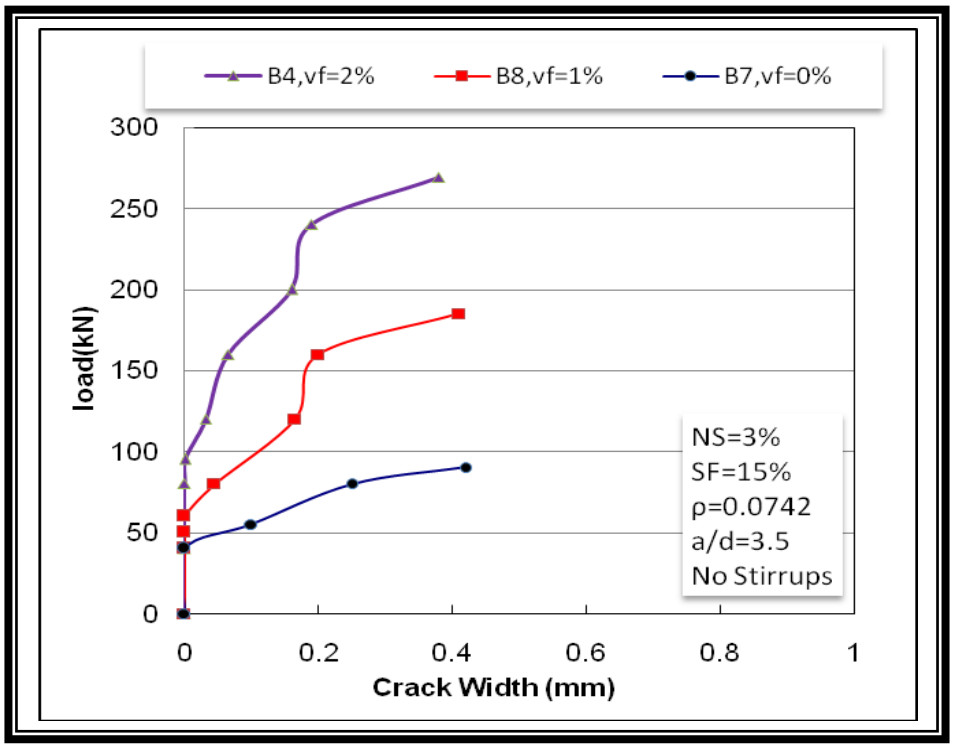

Fig. 4.33: Load-Crack Width Curves of NSRPC Beams (B7,B8, B4-Group 3)

Fig 4.34shows the effect of using higher longitudinal steel ratio ρ in the beam on the maximum crack width such that ρ= 0.0742 (B4), ρ= 0.0857 (B9) and ρ= 0.0911 (B10), belonging to group 4. It is clear from this figure that increasing ρ in the beam lead to an increase in the width of the shear crack at the onset of failure. This is due to the fact that the increase in ρ made the beam to resist higher ultimate load which was accompanied by a wider shear crack at failure.

Fig. 4.35 shows the effect of increasing the shear span to effective depth ratio a/d on the maximum crack width, represented by beams of group 5. It can be observed from this figure that increasing a/d ratio caused reduction in the shear crack width at the onset of shear failure and along all stages of loading. This is due to the fact that the increase in a/d ratio caused greater bending moment to develop in the beam and this made the beam to resist lower ultimate load and hence narrower crack width at failure.

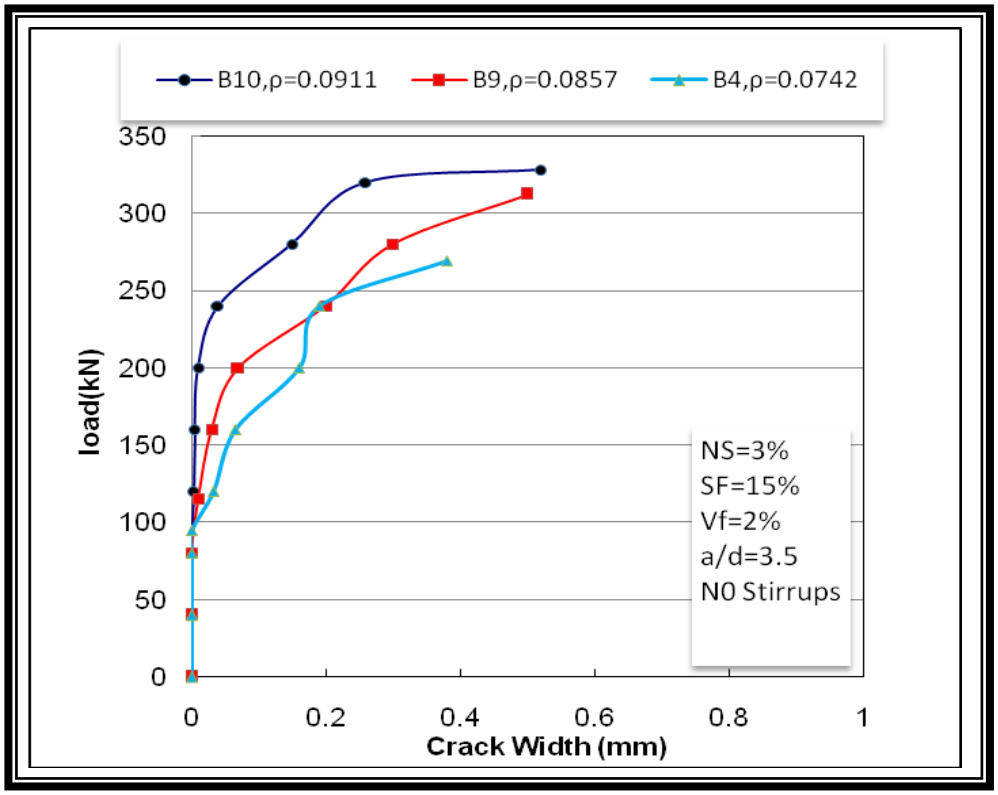

Fig. 4.34: Load-Crack Width Curves of NSRPC Beams (B4,B9,B10-Group 4)

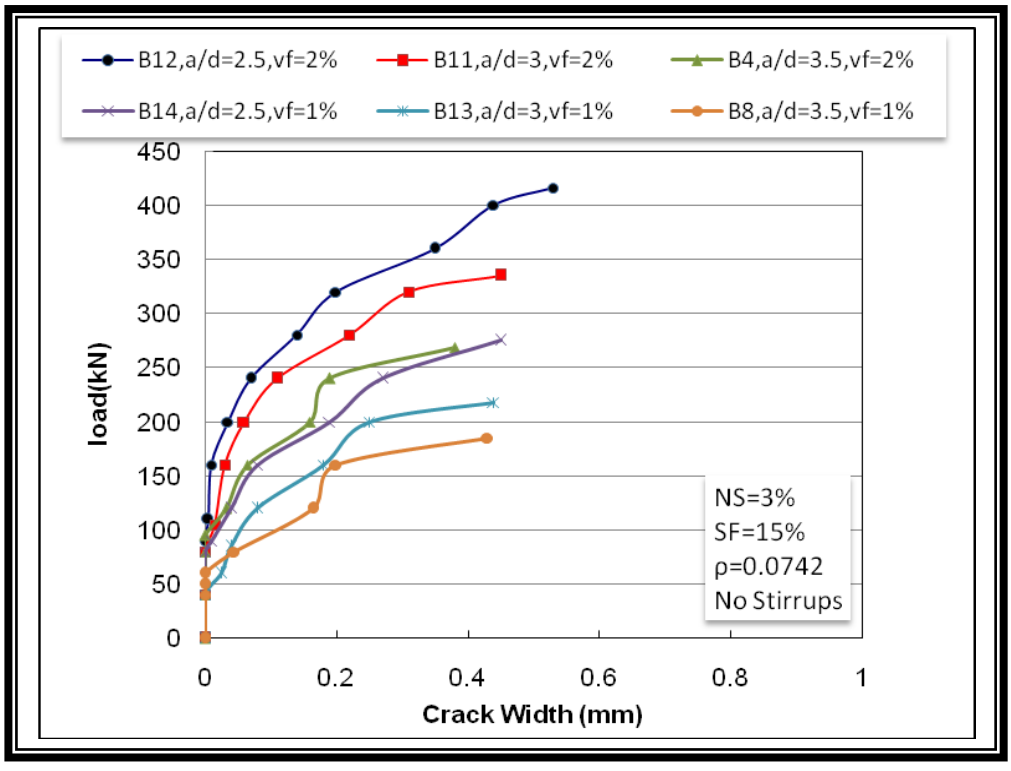

Fig. 4.35: Load-Crack Width Curves of NSRPC Beams (B4,B11,B12,B8,B13,B14-Group 5)

Fig 4.36 shows the effect of using steel stirrups in the beam on the maximum crack width. This is represented by group 6. It can be seen from this Figure that the use of steel stirrups in the beam increased the shear strength of the beam and reduced the crack width at all stages of loading as well as at the onset of failure.

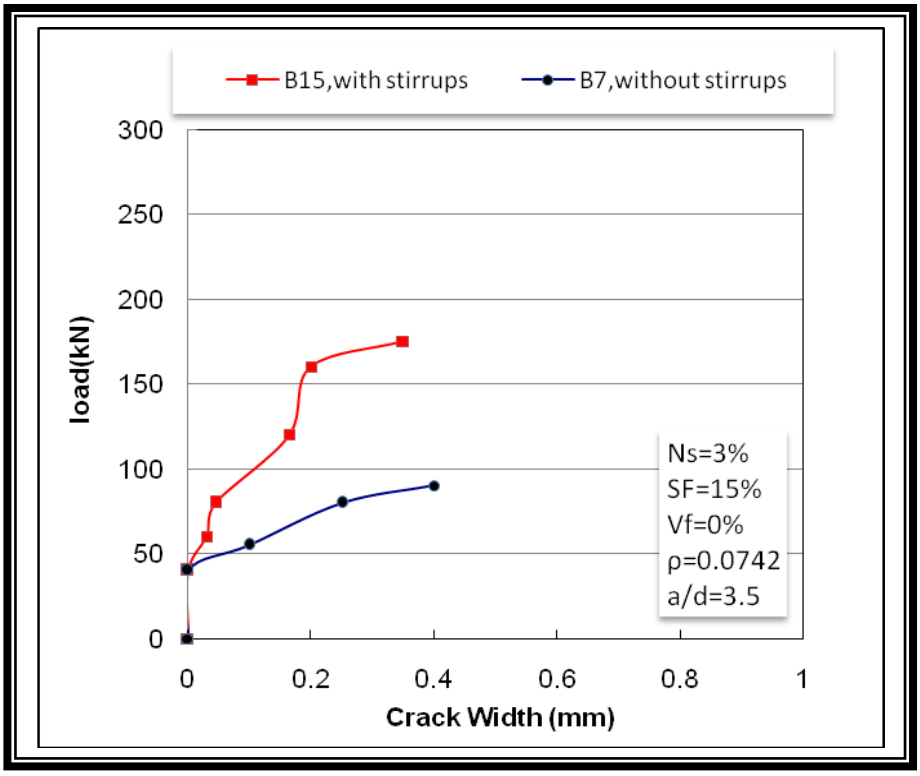

Fig. 4.36: Load-Crack Width Curves of NSRPC Beams (B7,B15 -Group 6)

Fig 4.37 shows the effect of the dual absence of nanosilica and steel fibers in the beam on the maximum crack width. This is represented by group 7 . It is clear from this figure that the absence of both NS and V_f in B16 resulted in a wider shear cracks width at all stages of loading and at failure compared with that of B4.

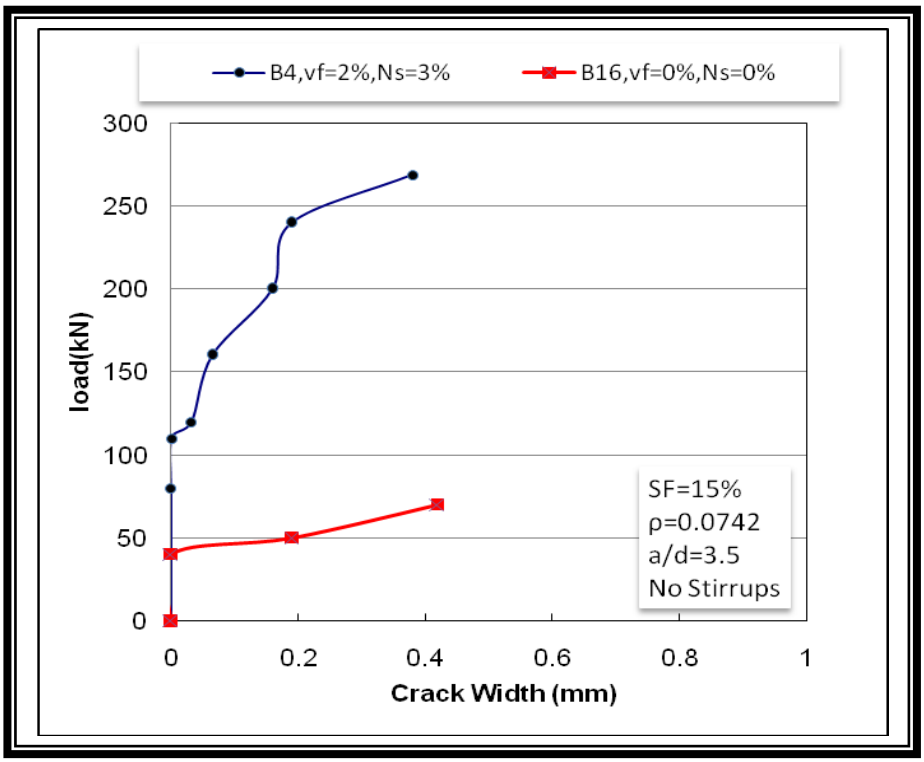

Fig. 4.37: Load-Crack Width Curves of NSRPC Beams (B4,B16 -Group 7)

4-7 Load- Concrete Strain Relationships

Two types of concrete strains were measured for each tested NSRPC beam of the present investigation. These are:

1. Longitudinal tensile strains ε_L at the level of the longitudinal steel bars (i.e at C.G of As). These longitudinal tensile strains were measured at different sections across the total length of the beam using demic gauges. The gage length between two adjacent demec points was 150mm as shown in Fig .3.9 of the preceding chapter. Eight gage lengths labeled a,b,c,d,e,f,g and h were used with the center of the outer gage lengths (a) and (h) located 175mm from the nearer beam support and that the border line between the two middle gage lengths (d) and (e) coincided with the mid-span section of the beam.

It was aimed from these longitudinal tensile strains ε_L to draw a longitudinal strain distribution along the full length of the beam at any load level and to find out whether the steel bars yielded or not when the beam collapsed had or had not reached yield.

2. Diagonal splitting tensile strain ε_D in the direction perpendicular to the expected diagonal tension crack (which, the crack, was found to extend from the beam support to the nearer applied concentrated load).As shown in Fig. 3.9 of Chapter 3, two diagonal splitting tensile strains ε_D were measured in each shear span of the beam using 100mm demec gauges. One diagonal strain was at mid of the shear span at mid- depth (labeled strain 1-1 in the left shear span and strain 4-4 in the right shear span) and the second diagonal strain was measured at 100 mm distance away from the mid- depth diagonal strain via the applied concentrated load (labeled strain 2-2 in the left shear span and strain 3-3 in the right shear span).

It was aimed from these diagonal splitting tensile strains ε_D to detect the degree of their variation with load and to record their maximum value at the onset of beam collapse.

Fig. 4.38 to 4.51 show the distribution of the longitudinal tensile strains ε_L (measured at C.G level of steel bars) along the full length of the tested NSRPC beams B1 to B16. In each figure, a set of curves were drawn such that one curve represents the values of the eight ε_L strains corresponding to a specified magnitude of the applied load. The variations were shown throughout the whole loading history up to beam collapse.

In addition, Table 4.9 lists the maximum value of the longitudinal tensile strains in concrete $\varepsilon_{L\ max}$ (measured at C.G level of steel bars) for each specified value of the applied load up to beam collapse. The Table covers the output obtained for all the sixteen tested NSRPC beams of this research. It can be seen from this table that the maximum value of such

longitudinal tensile strains $\varepsilon_{L\ max}$ (obtained at the onset of beam collapse) was found within the range (3152 με to 4706 με). This assured the yielding of the steel bars since the yield strain of the 28mm diameter steel bars= 2590 με and that of the 12 mm diameter steel bars= 3050 με (as given in Table 3-12 of chapter three).

Figs. 4.54 to 4.66 show the variation of the diagonal splitting tensile strains ε_D 1-1, 2-2, 3-3 and 4-4 with the applied load for all the sixteen tested NSRPC beams. Table 4.10 lists the maximum value of the diagonal tensile strain in concrete $\varepsilon_{D\ max}$ for each specified value of the applied load up to beam collapse. It must be pointed out here that there was some inconsistency in the data obtained for these ε_D strains at the final stages of loading prior to collapse because of the widening of the diagonal splitting tension cracks within the region of these inclined strain gages.

The following observations were detected from the measurements of the maximum longitudinal tensile strains ε_{Lmax} and maximum diagonal tensile strains ε_{Dmax}

1. At the same load level, the values of ε_{Lmax} and ε_{Dmax} decrease consistently as the percentage of nanosilica NS increases. For example at load 160 kN, increasing NS from 0% (B1) to 1% (B2), 2% (B3) and 3%(B4) led to a decrease in ε_{Lmax} of 12.4%, 18.8% and 21.6% respectively and a decrease in ε_{Dmax} of 53.3 %,55.1 % and73.8 % respectively.
2. Also that at load 160 kN (for example) increasing the percentage of silica fume from 5% (B5) to 10% (B6) and 15% (B4) led to a decrease in ε_{Lmax} of 7.5% and 11.0% respectively and a decrease in ε_{Dmax} of 9.6 % and 15.4% respectively.
3. The increase in the percentage of the volumetric ratio of steel fibers V_f was also found to reduce the value of the maximum tensile longitudinal strain ε_{Lmax} and maximum diagonal tensile strain ε_{Dmax} at any load level.

At load 160 kN increasing V_f from 1% (B8) to 2% (B4) caused a reduction in ε_{Lmax} of 20% and a dramatic reduction in ε_{Dmax} of 78%. This assured the beneficial effect of steel fibers in increasing the splitting tensile strength of the nanosilica reactive powder concrete and enable it to withstand higher diagonal tensile stress with only little diagonal tensile stain. It can be argued that the steel fibers acted as a crack arrester until when shear (or diagonal tension) failure occurred the steel fibers were seen to pull out of the concrete solid matrix without rupture.

4. The increase in the longitudinal steel ratio ρ gave an additional cause for the reduction in the concrete strains $\varepsilon_L$and ε_D at any level. For example at load 160 kN increasing ρ from 0.0742 (B4) to 0.0857 (B9) and 0.0911 (B10) caused a reduction in ε_{Lmax} of 39.8% and 40.9% respectively but only little reduction in ε_{Dmax} of 5.9% and 60.5% respectively. This is reasonable since the contribution of longitudinal steel bars in flexural strength is usually much higher than its contribution in shear resistance.
5. The increase in the shear span to effective depth ratio a/d resulted in an increase in both ε_{Lmax} and ε_{Dmax} at the same load level. For example at load 240kN increasing a/d from 2.5(B12) to 3 (B11) and 3.5 (B4) caused an increase in ε_{Lmax} of 0.7% and 82% respectively and an increase in ε_{Dmax} of 405% and 847% respectively. This is due to the fact that the increase in a/d ratio caused greater bending moment to develop in the beam and hence gave greater tensile stresses and tensile strains.

However, the reverse effects were seen at the onset of shear failure of these beams; increasing a/d ratio from 2.5 (B12) to 3 (B11) and 3.5 (B4) caused a reduction in ε_{Lmax} of 17.5% and 19.1% respectively and a reduction in ε_{Dmax} of 10.5% and 50% respectively. This can be attributed to the decrease in the value of ultimate load of beams B11 and B4 compared to beam B12 and this reduction in ultimate load resulted in a subsequent

reduction in the maximum values of the longitudinal tensile strain ε_{Lmax} and diagonal splitting tensile strain ε_{Dmax}.

6. The use of steel stirrups in beam (B15) enabled the beam to resist greater ε_{Dmax} at failure than its relevant beam (B7) without steel stirrups, but ε_{Lmax} very little increased . The percentage increase in both ε_{Dmax} and ε_{Lmax} were of the order 47% and 3.6% respectively . Such increases were reasonable because steel stirrups did help in providing extra tensile stiffness in the two shear spans of beam B15, but had only little effect on ε_{Lmax} .
7. The dual absence of nanosilica and steel fibers from the concrete mix made the beam to undergo greater ε_{Lmax} and ε_{Dmax} at a specified load level. A comparison of these strains in beam B16 (NS=0% ,Vf=0%) with those of beam B4 (NS=3%, Vf=2%) at a load 40 kN (for example) shows that ε_{Lmax} was increased by 164% while ε_{Dmax} was increased by 480%. It was found that the absence of steel fibers had a greater influence in increasing these strains than did the absence of nanosilica.

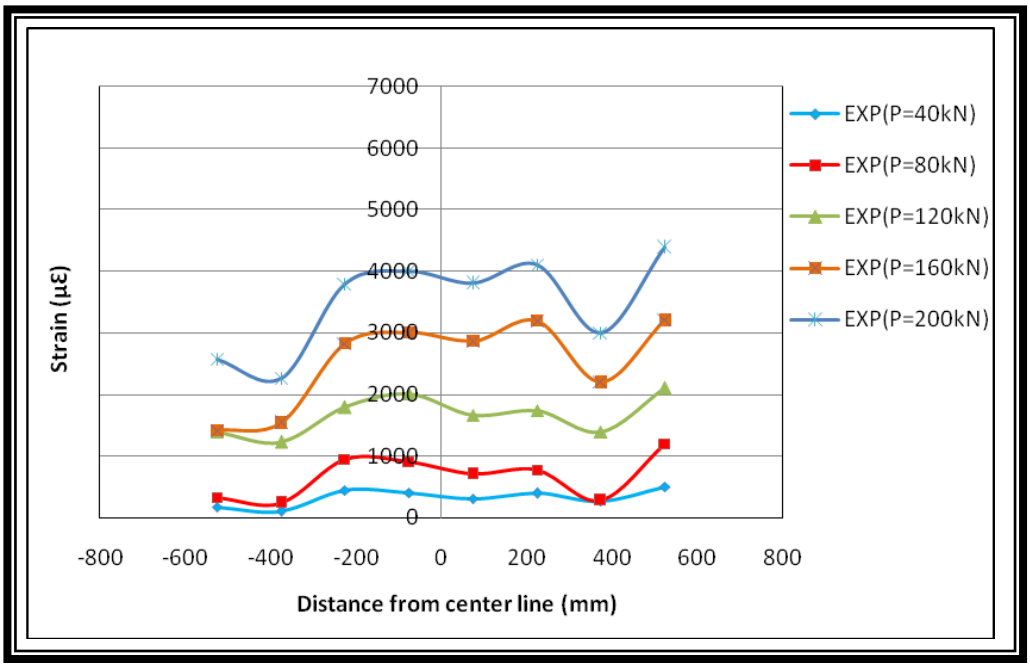

Fig. 4.38:Distribution of Longitudinal Tensile Strains ε_L at C.G Level of Steel Bars of NSRPC Beam B1

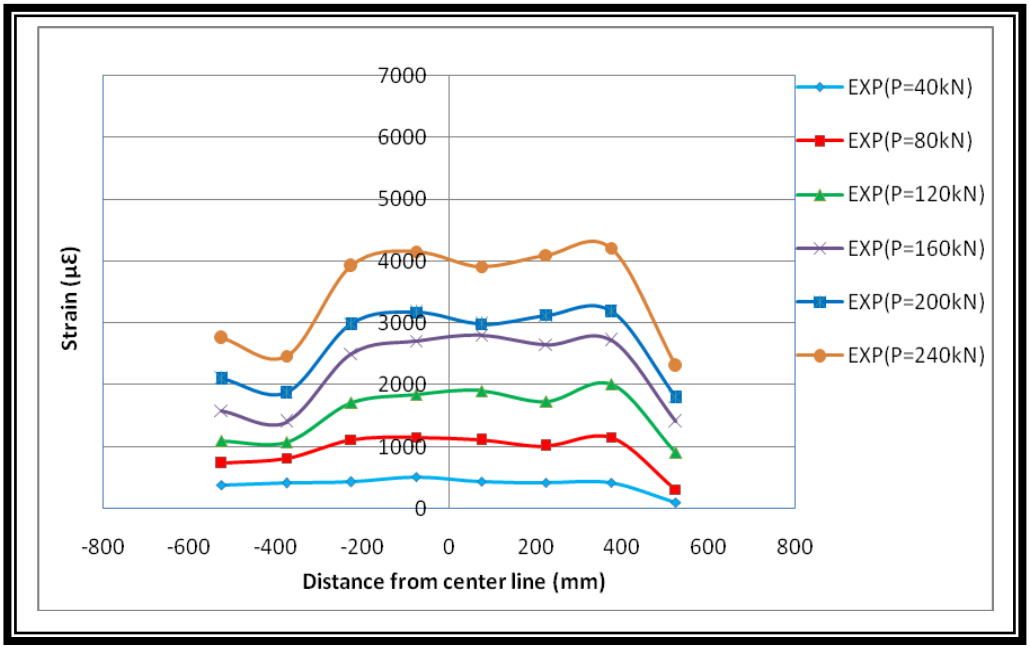

Fig. 4.39:Distribution of Longitudinal Tensile Strains ε_L at C.G Level of Steel Bars of NSRPC Beam B2

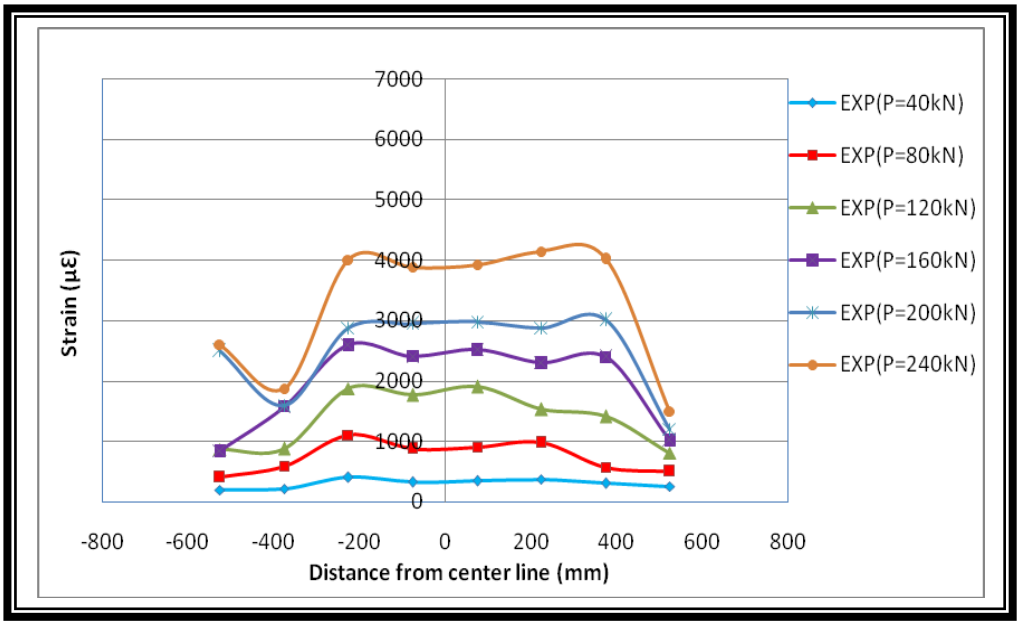

Fig. 4.40:Distribution of Longitudinal Tensile Strains ε_L at C.G Level of Steel Bars of NSRPC Beam B3

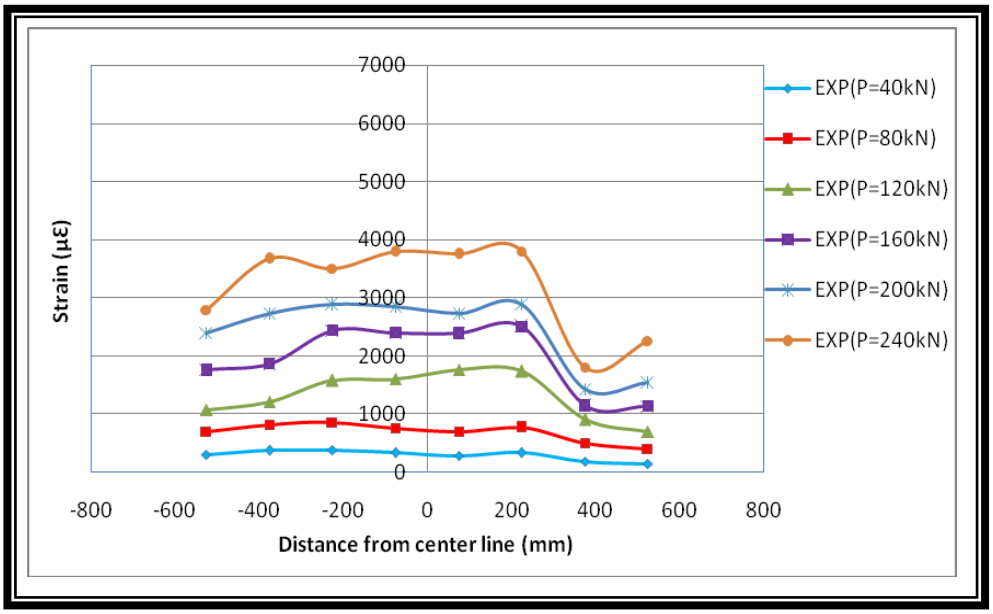

Fig. 4.41:Distribution of Longitudinal Tensile Strains ε_L at C.G Level of Steel Bars of NSRPC Beam B4

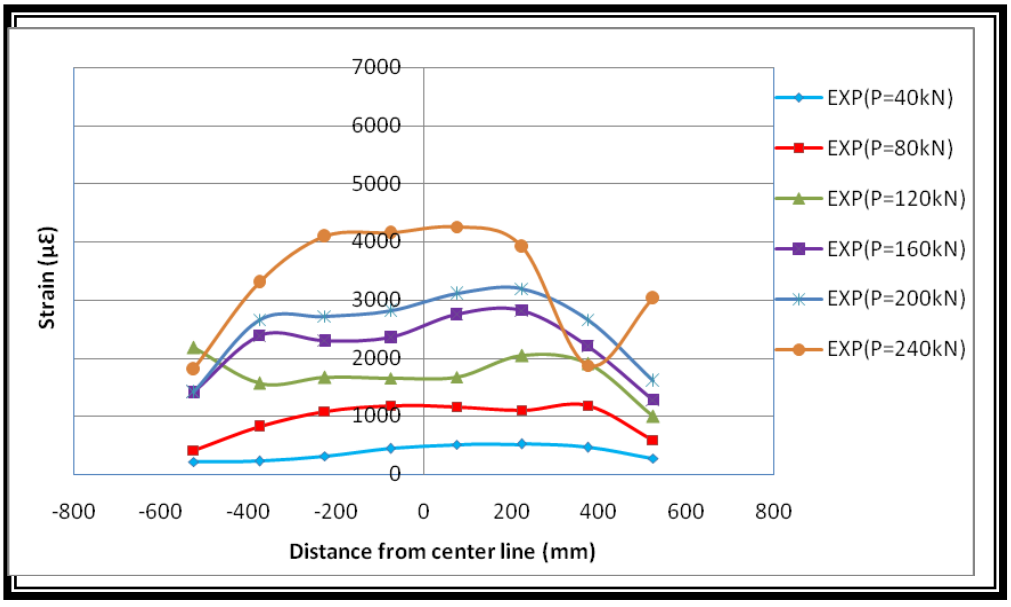

Fig. 4.42:Distribution of Longitudinal Tensile Strains ε_L at C.G Level of Steel Bars of NSRPC Beam B5

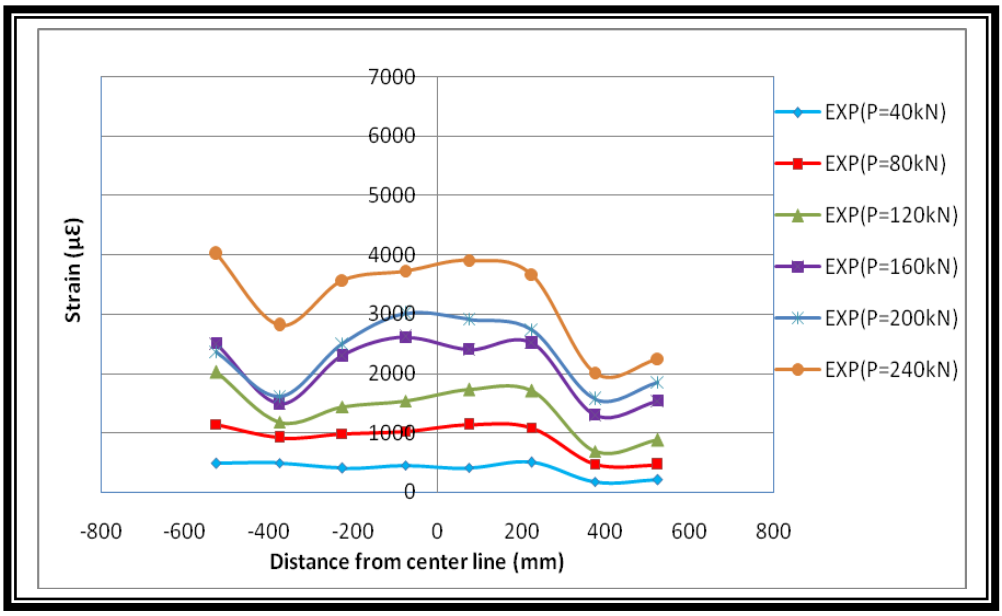

Fig. 4.43:Distribution of Longitudinal Tensile Strains ε_L at C.G Level of Steel Bars of NSRPC Beam B6

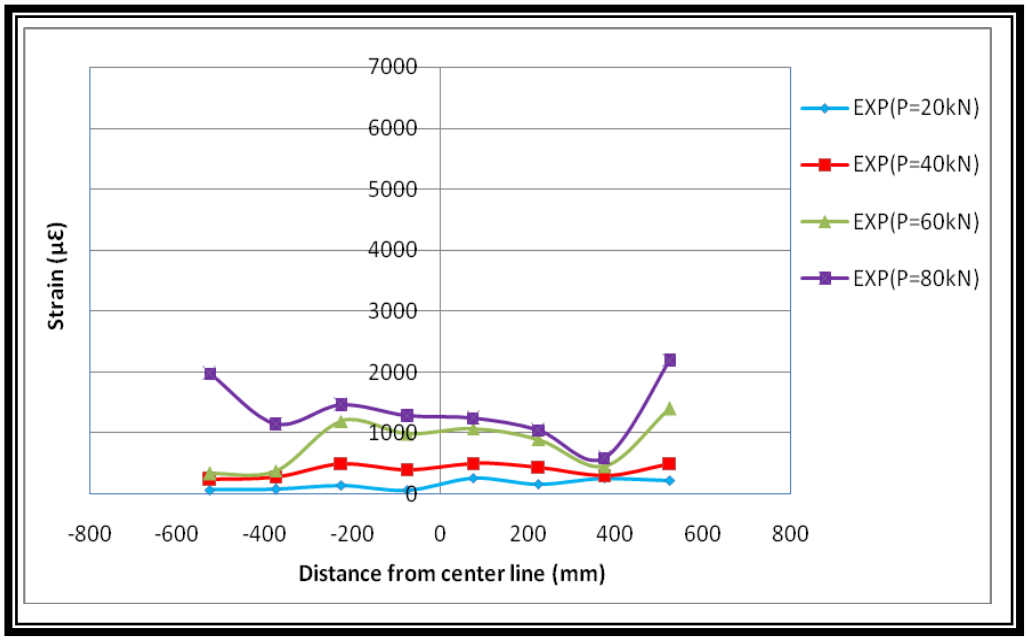

Fig. 4.44:Distribution of Longitudinal Tensile Strains ε_L at C.G Level of Steel Bars of NSRPC Beam B7

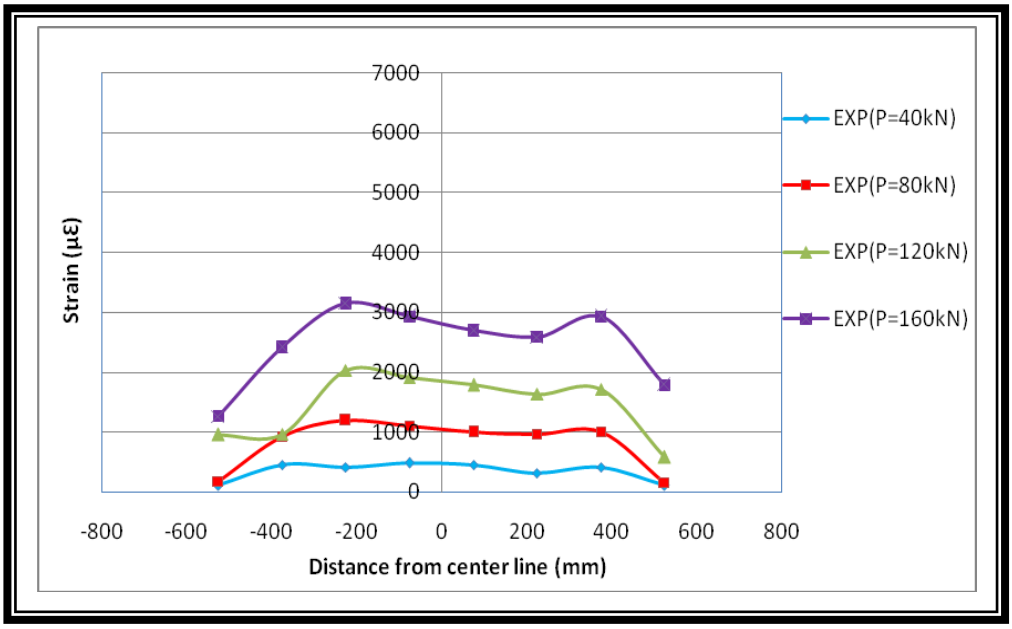

Fig. 4.45:Distribution of Longitudinal Tensile Strains ε_L at C.G Level of Steel Bars of NSRPC Beam B8

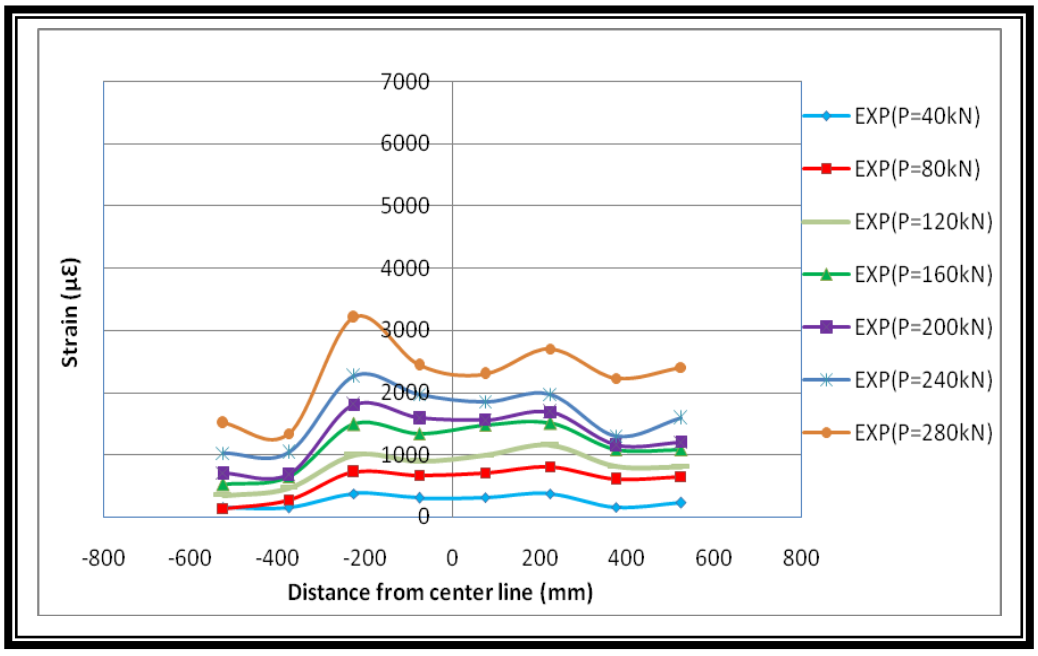

Fig. 4.46:Distribution of Longitudinal Tensile Strains ε_L at C.G Level of Steel Bars of NSRPC Beam B9

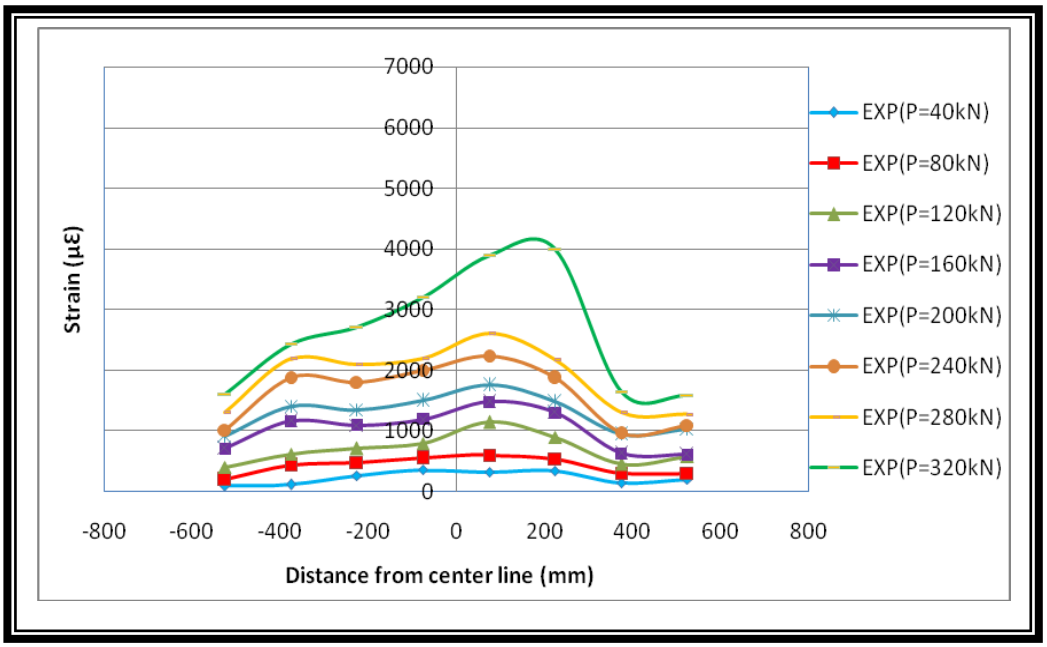

Fig. 4.47:Distribution of Longitudinal Tensile Strains ε_L at C.G Level of Steel Bars of NSRPC Beam B10

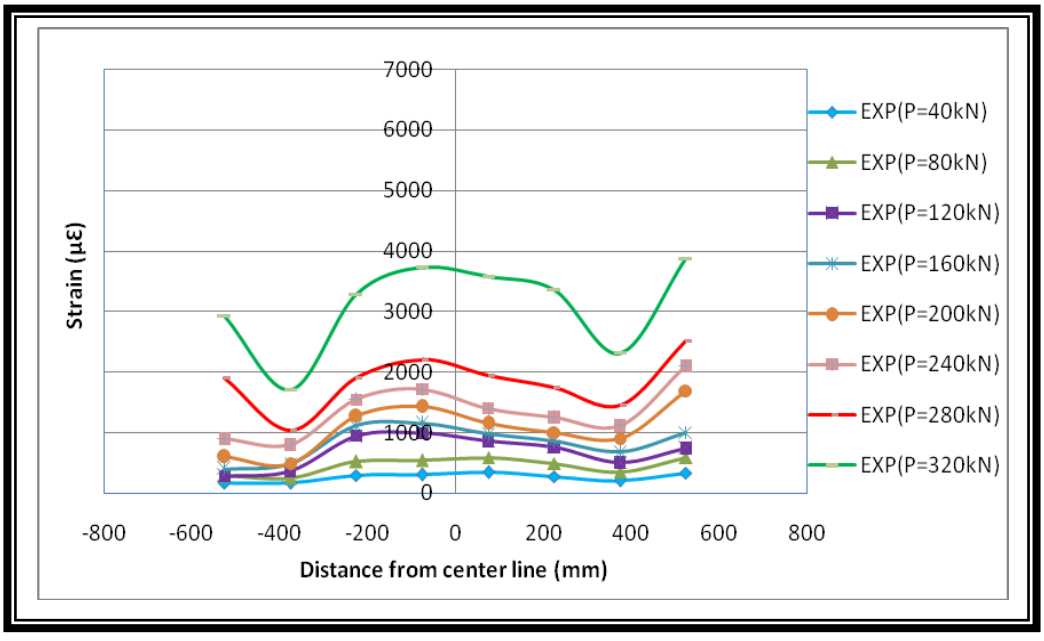

Fig. 4.48:Distribution of Longitudinal Tensile Strains ε_L at C.G Level of Steel Bars of NSRPC Beam B11

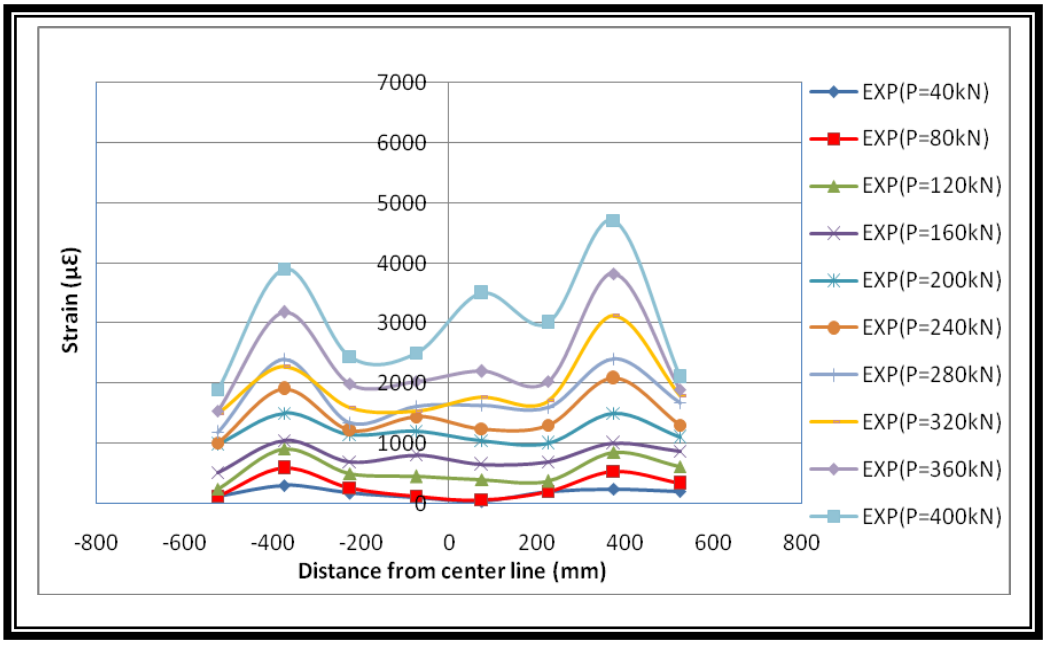

Fig. 4.49:Distribution of Longitudinal Tensile Strains ε_L at C.G Level of Steel Bars of NSRPC Beam B12

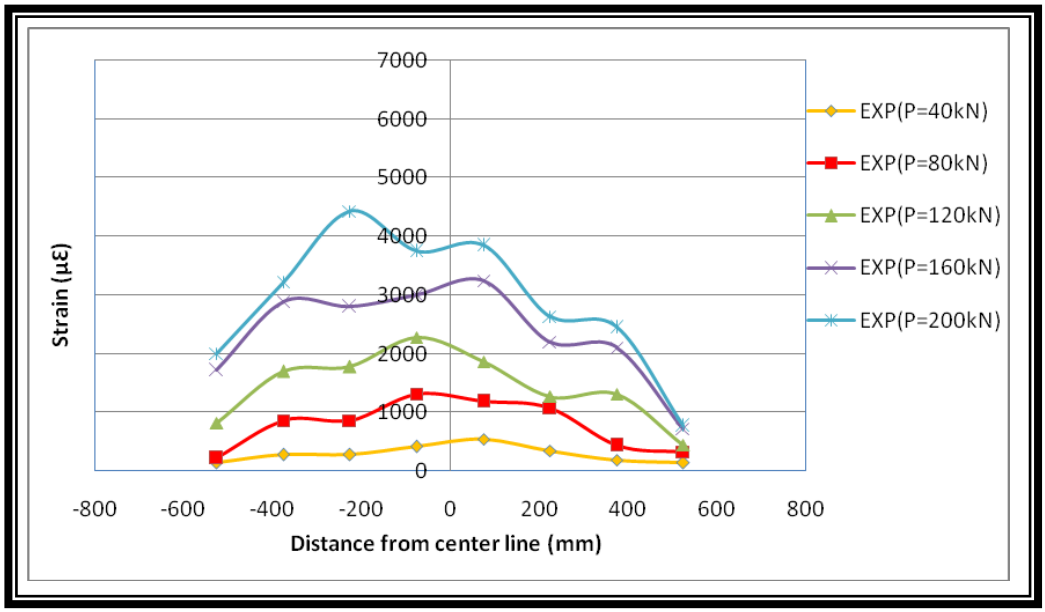

Fig. 4.50:Distribution of Longitudinal Tensile Strains ε_L at C.G Level of Steel Bars of NSRPC Beam B15

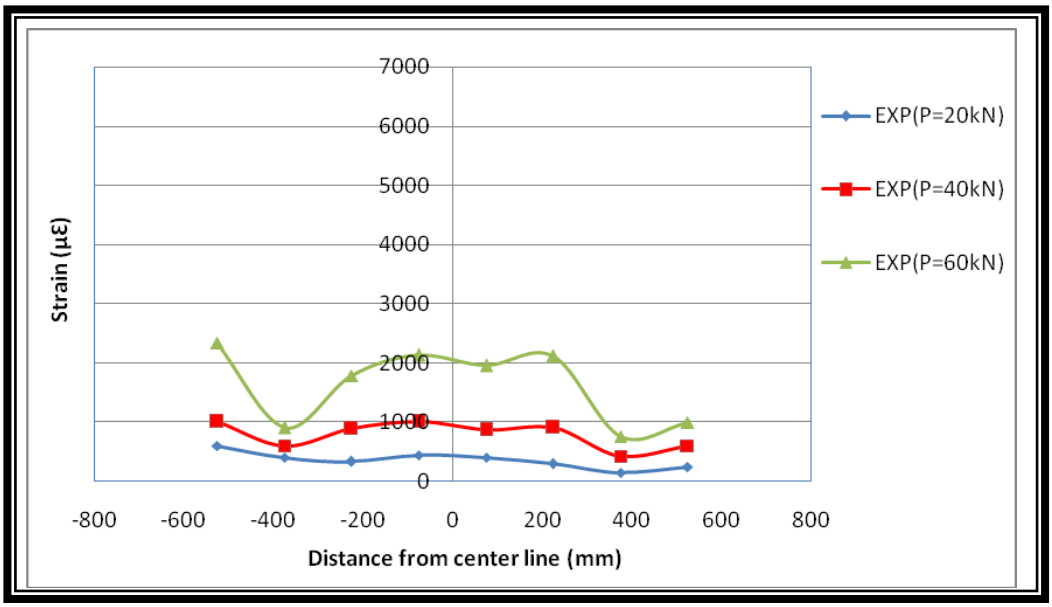

Fig. 4.51:Distribution of Longitudinal Tensile Strains ε_L at C.G Level of Steel Bars of NSRPC Beam B16

Table 4.9 Values of ε_{Lmax} at Different Load Levels of the Tested NSRPC Beams

Beam	Micro Strain@ Load											
	20 kN	40 kN	60 kN	80 kN	120 kN	160 kN	200 kN	240 kN	280 kN	320 kN	360 kN	400 kN
B1		504		1200	2100	3200	3387					
B2		509		1154	2010	2803	3190	4155				
B3		405		1104	1902	2600	3010	4150				
B4		383		862	1763	2510	2890	3803				
B5		460		1181	2175	2821	3195	4255				
B6		502		1140	2022	2610	3010	4015				
B7	265	510	1403	2201								
B8		478		1190	2026	3152						
B9		381		805	1156	1512	1803	2260	3204			
B10		361		609	1151	1484	1757	2242	2610	4001		
B11		342		590	993	1150	1690	2103	2505	3878		
B12		250		543	910	1050	1506	2089	2414	3127	3829	4706
B15		540		1312	2280							
B16	600	1011	2340									

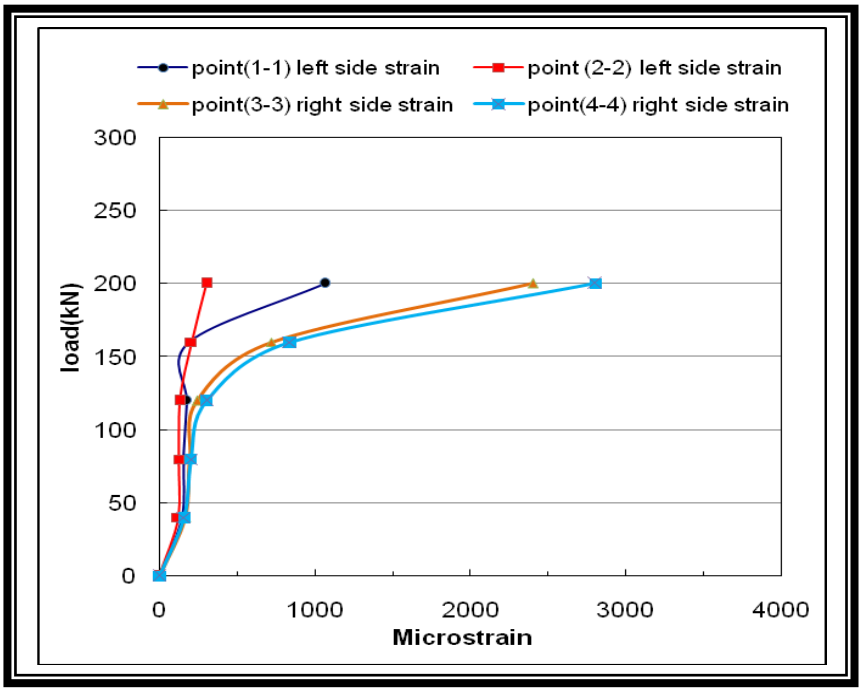

Fig. 4.52:Load Versus Diagonal Splitting Tensile Strains ε_D for B1

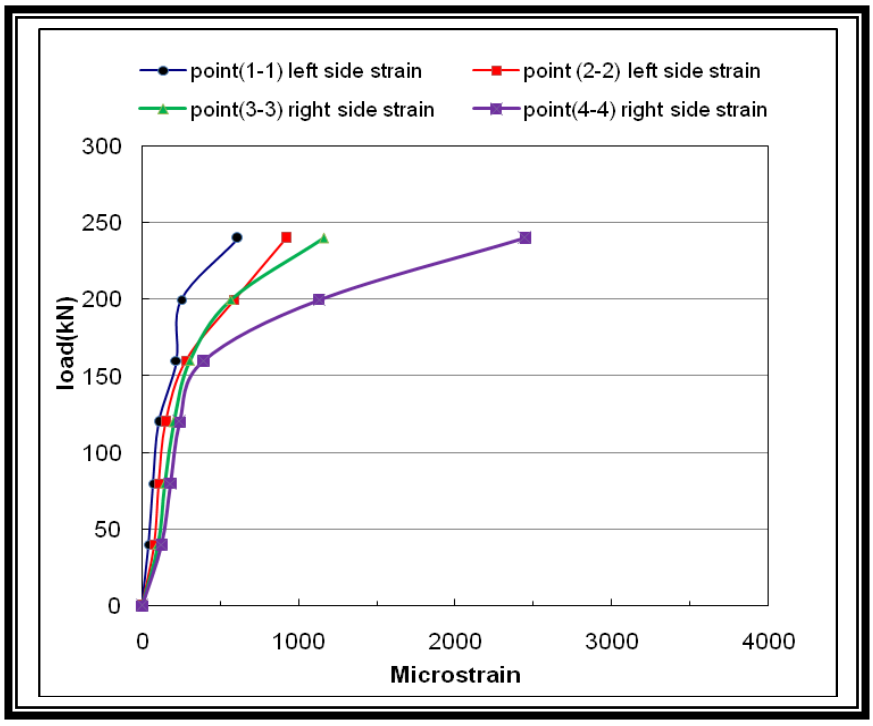

Fig. 4.53:Load Versus Diagonal Splitting Tensile Strains ε_D for B2

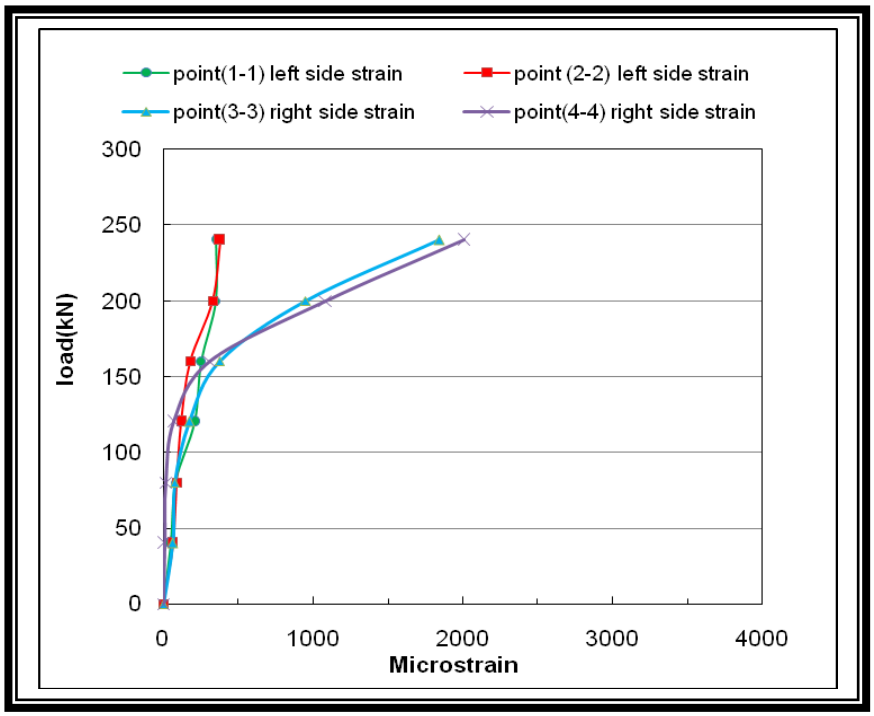

Fig. 4.54:Load Versus Diagonal Splitting Tensile Strains ε_D for B3

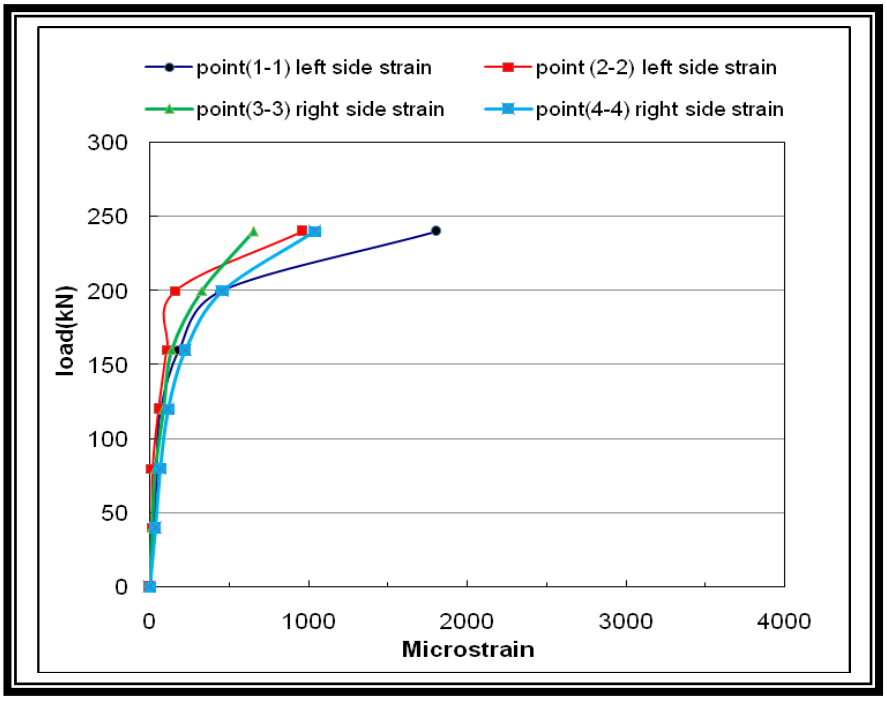

Fig. 4.55:Load Versus Diagonal Splitting Tensile Strains ε_D for B4

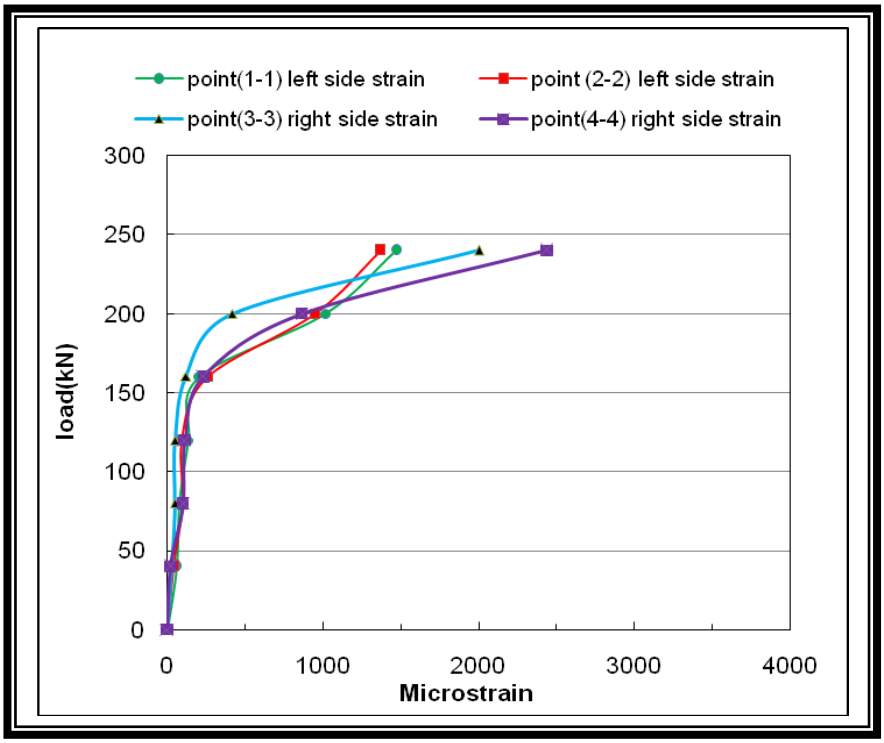

Fig. 4.56:Load Versus Diagonal Splitting Tensile Strains ε_D for B5

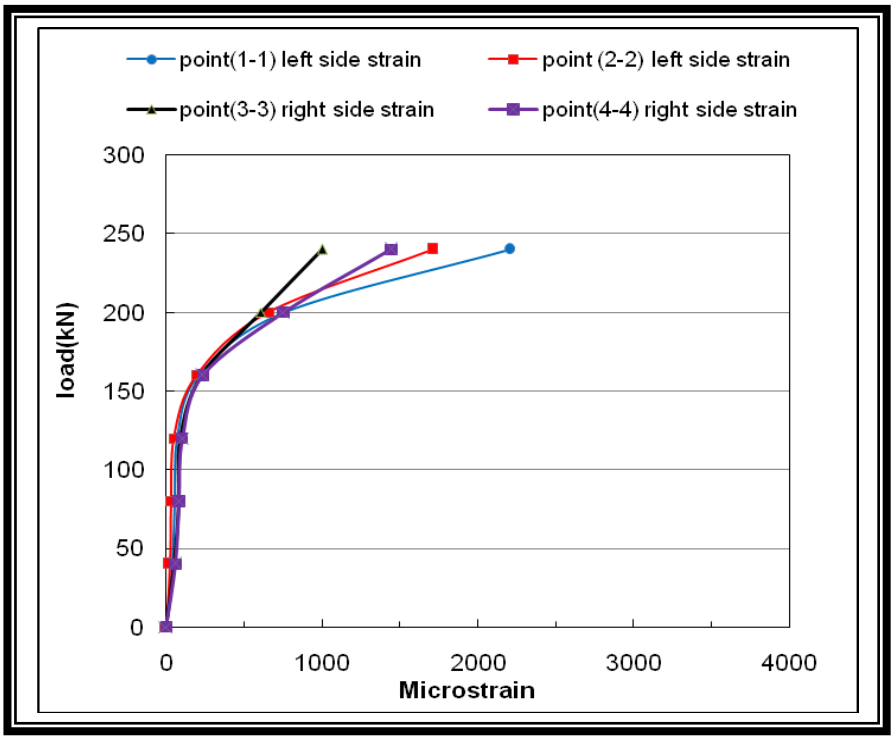

Fig. 4.57:Load Versus Diagonal Splitting Tensile Strains ε_D for B6

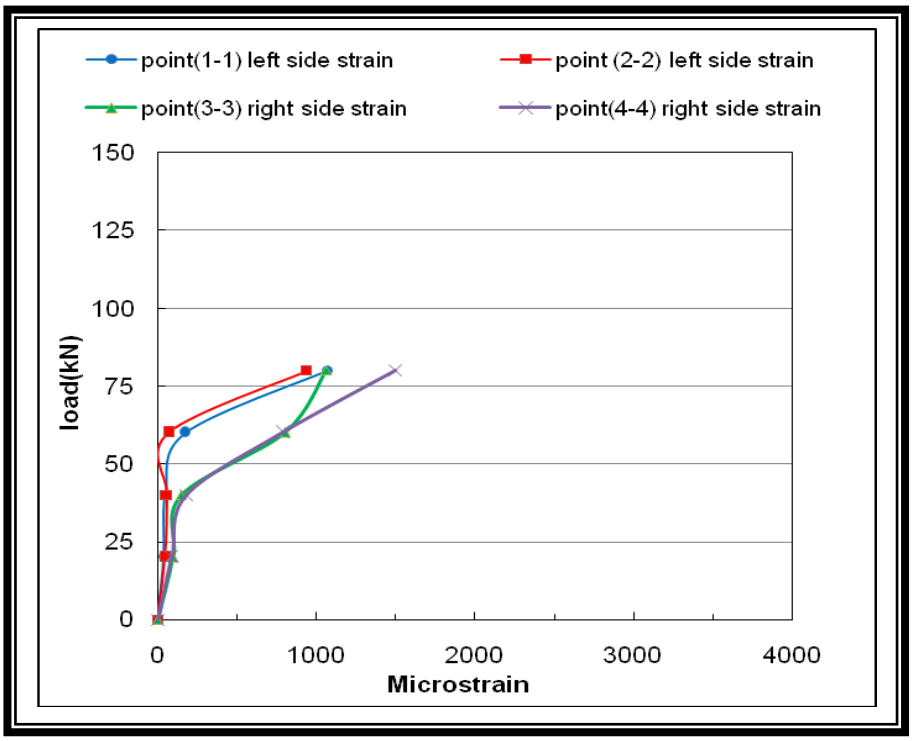

Fig. 4.58:Load Versus Diagonal Splitting Tensile Strains ε_D for B7

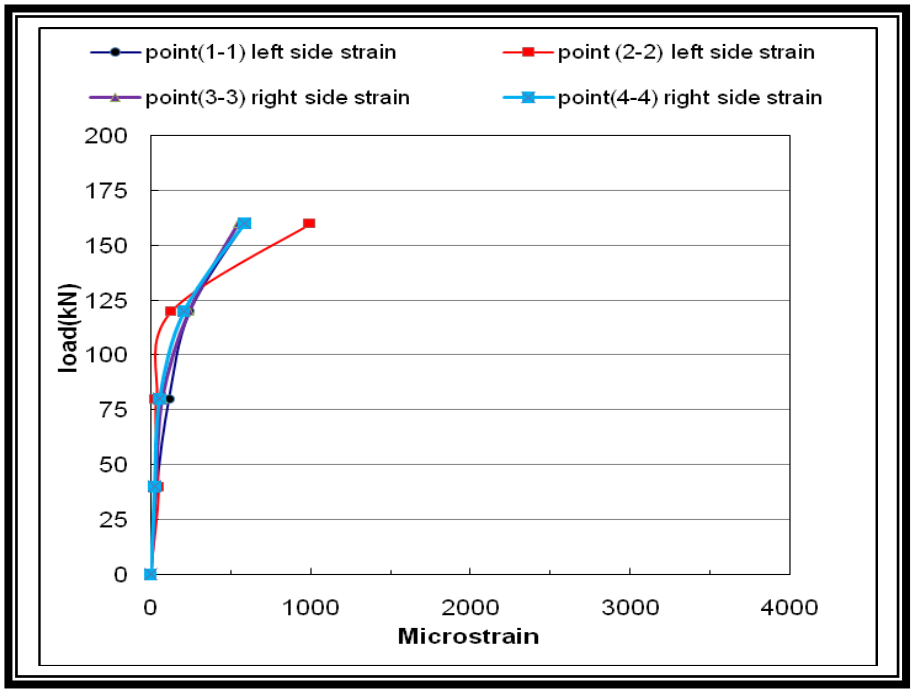

Fig. 4.59:Load Versus Diagonal Splitting Tensile Strains ε_D for B8

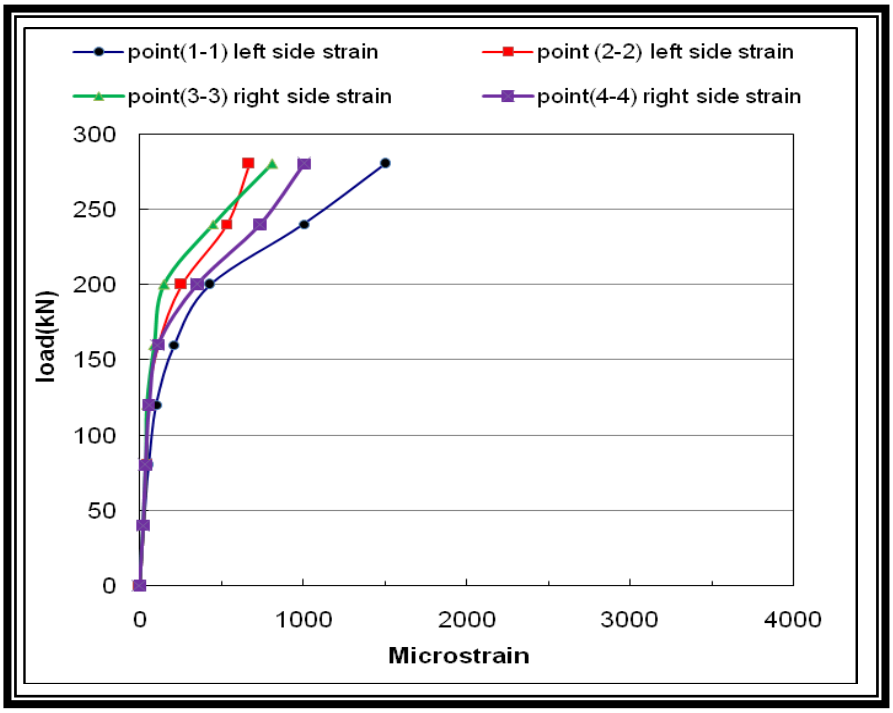

Fig. 4.60:Load Versus Diagonal Splitting Tensile Strains ε_D for B9

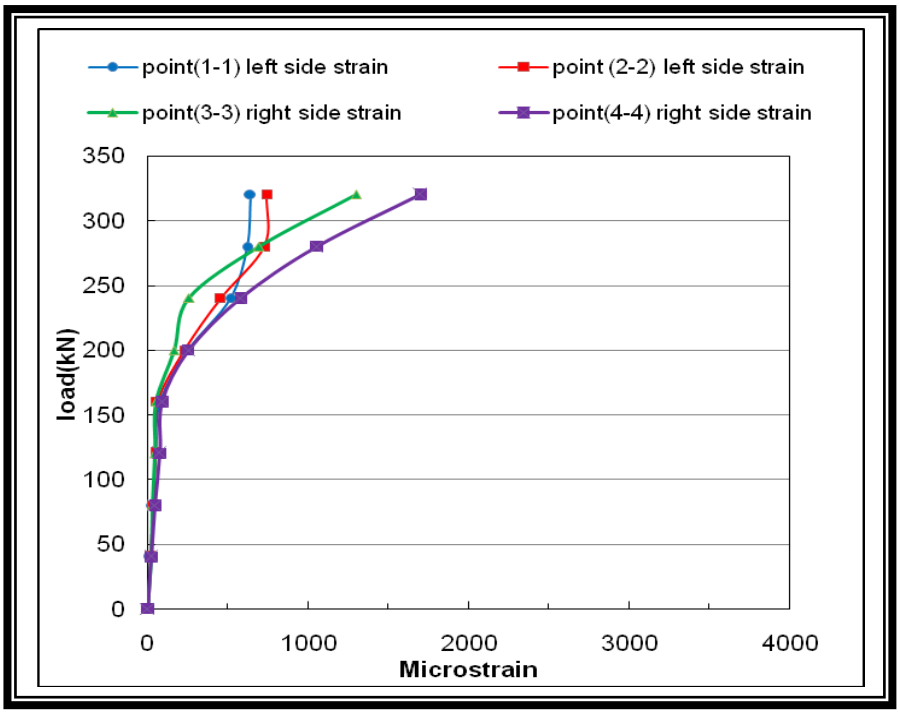

Fig. 4.61:Load Versus Diagonal Splitting Tensile Strains ε_D for B10

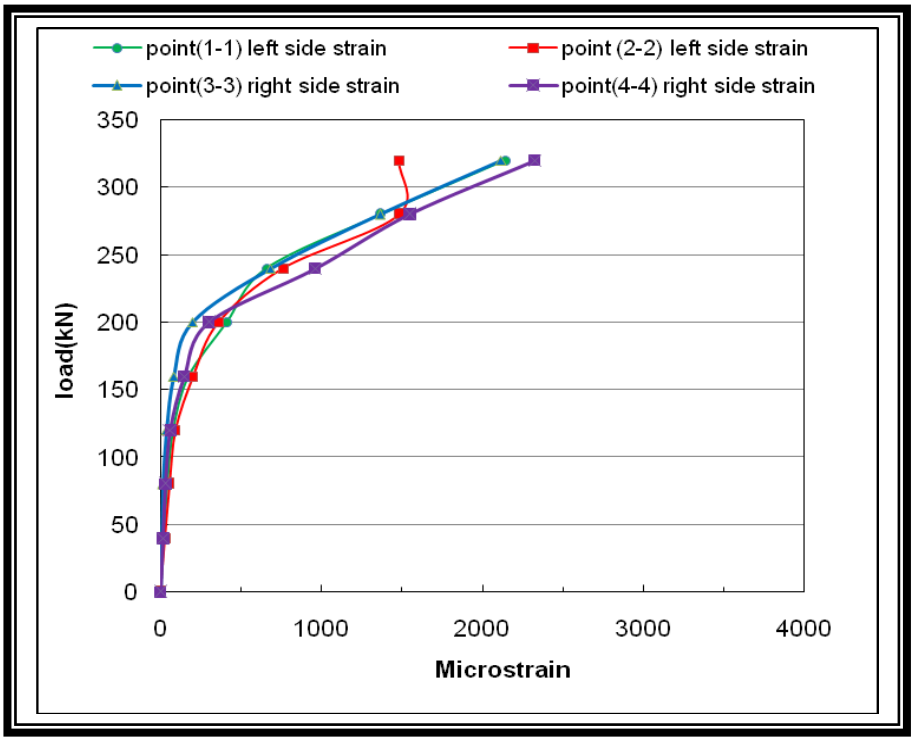

Fig. 4.62:Load Versus Diagonal Splitting Tensile Strains ε_D for B11

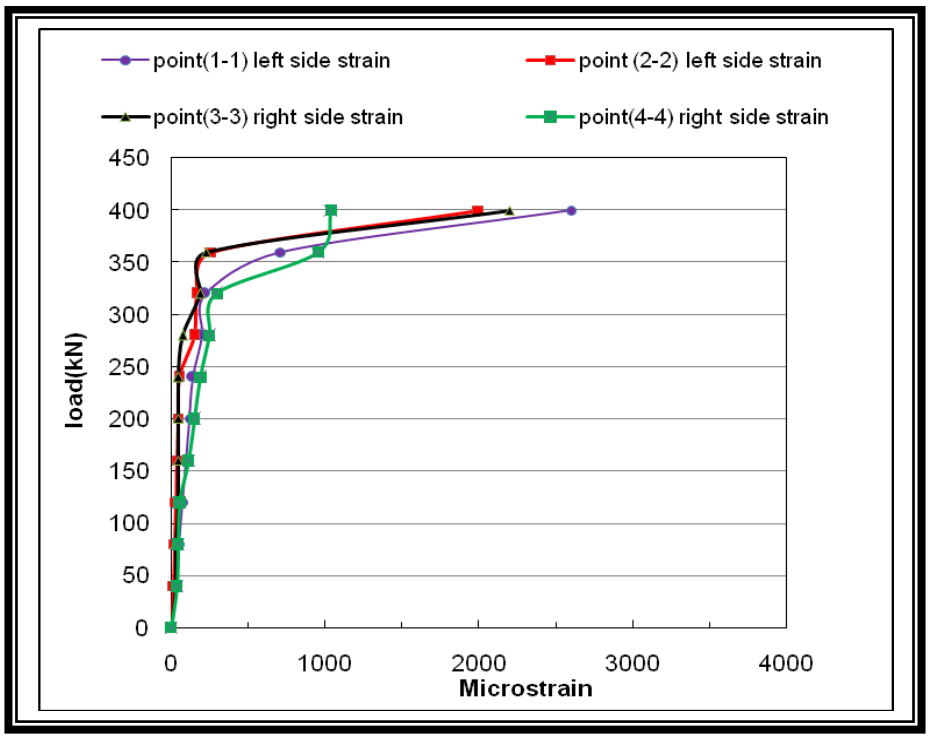

Fig. 4.63:Load Versus Diagonal Splitting Tensile Strains ε_D for B12

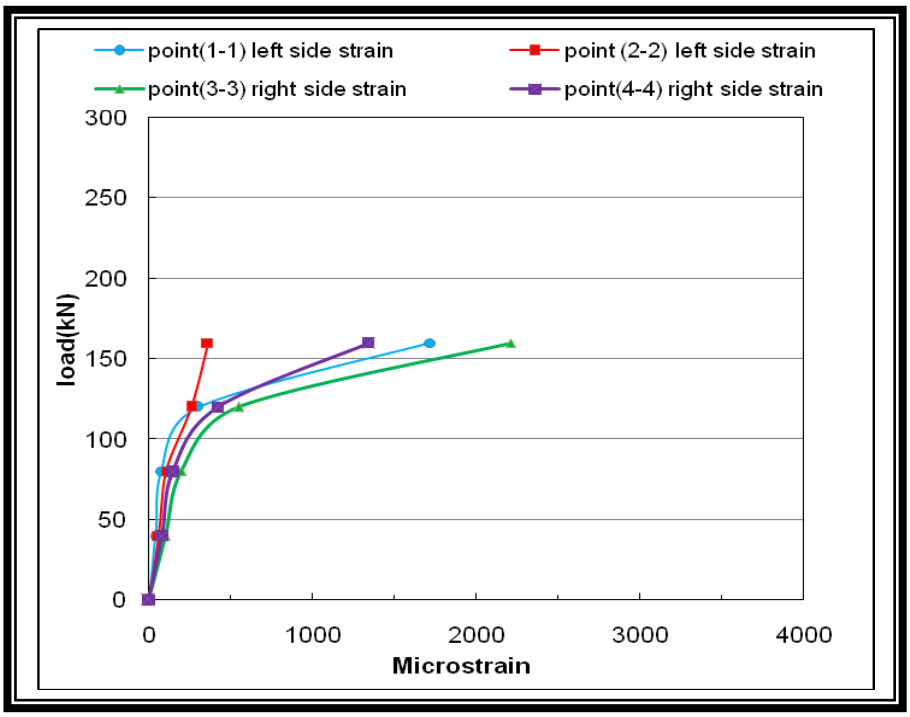

Fig. 4.64:Load Versus Diagonal Splitting Tensile Strains ε_D for B15

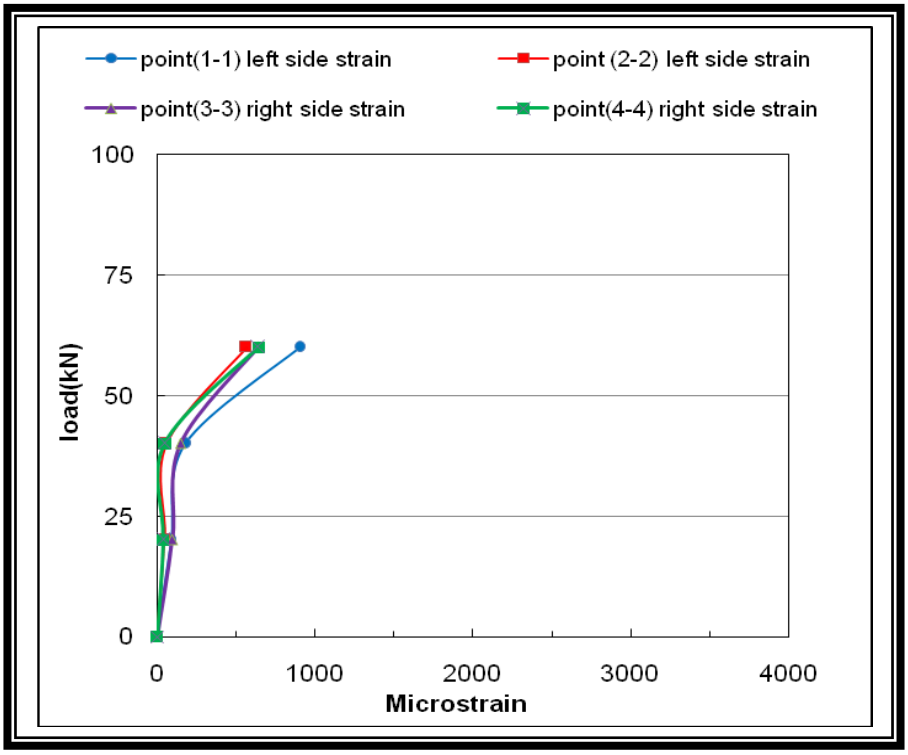

Fig. 4.65:Load Versus Diagonal Splitting Tensile Strains ε_D for B16

Table 4.10 Values of εDmax at Different Load Levels of the Tested NSRPC Beams

Beam	Micro Strain@ Load											
	20 kN	40 kN	60 kN	80 kN	120 kN	160 kN	200 kN	240 kN	280 kN	320 kN	360 kN	400 kN
B1		167		202	304	839	2804					
B2		125		182	242	391	1130	2450				
B3		65		92	211	377	1086	2005				
B4		31		62	115	220	456	1800				
B5		60		100	135	260	1016	2438				
B6		36		80	100	235	758	2200				
B7	95	170	787	1500								
B8		50		116	292	1000						
B9		25		50	100	207	425	1003	1500			
B10		20		45	74	187	250	580	1050	1700		
B11		28		54	92	203	410	961	1550	2325		
B12		40		55	75	113	150	190	250	300	957	2600
B15		100		200	550	2210						
B16	100	180	904									